

A study of high proper-motion white dwarfs

I. Spectropolarimetry of a cool hydrogen-rich sample^{*}

Adéla Kawka[†] and Stéphane Vennes[†]

Astronomický ústav AV ČR, Fričova 298, CZ-251 65 Ondřejov, Czech Republic

Accepted; Received

ABSTRACT

We conducted a spectropolarimetric survey of 58 high proper-motion white dwarfs which achieved uncertainties of $\gtrsim 2$ kG in the H α line and $\gtrsim 5$ kG in the upper Balmer line series. The survey aimed at detecting low magnetic fields ($\lesssim 100$ kG) and helped identify the new magnetic white dwarfs NLTT 2219, with a longitudinal field $B_1 = -97$ kG, and NLTT 10480 ($B_1 = -212$ kG). Also, we report the possible identification of a very low-field white dwarf with $B_1 = -4.6$ kG. The observations show that $\approx 5\%$ of white dwarfs harbour low fields (~ 10 to $\sim 10^2$ kG) and that increased survey sensitivity may help uncover several new magnetic white dwarfs with fields below ~ 1 kG. A series of observations of the high field white dwarf NLTT 12758 revealed changes in polarity occurring within an hour possibly associated to an inclined, fast rotating dipole. Also, the relative strength of the π and σ components in NLTT 12758 possibly revealed the effect of a field concentration (“spot”), or, most likely, the presence of a non-magnetic white dwarf companion. Similar observations of NLTT 13015 also showed possible polarity variations, but without a clear indication of the timescale. The survey data also proved useful in constraining the chemical composition, age and kinematics of a sample of cool white dwarfs as well as in constraining the incidence of double degenerates.

Key words: stars: fundamental parameters – stars: magnetic field – white dwarfs

1 INTRODUCTION

Magnetic fields in white dwarfs show great diversity in strength and structure. Field strengths from a few kilogauss (e.g., 40 Eri B or LTT 9857, Fabrika et al. 2000; Aznar Cuadrado et al. 2004) to nearly 10^9 G (e.g., J0317–855, Barstow et al. 1995; Ferrario et al. 1997) delineate the current range of detection, although higher and lower fields cannot, in principle, be ruled out. Low-dispersion spectropolarimetric surveys successfully achieved detection limits below a kilogauss (Aznar Cuadrado et al. 2004) or of the order of a few kG (Schmidt & Smith 1994; Kawka et al. 2007), while echelle spectroscopy achieved limits of several kilogauss with Zeeman splitting measurements in line cores (Koester et al. 1998). The spectra of high-field white dwarfs are very complex and detailed modelling requires application of model atoms in high-fields (Martin & Wickramasinghe 1984; Jordan 1992). Hydrogen and helium atomic data are

available for such studies (Kemic 1974; Garstang & Kemic 1974).

Stellar rotation, by exposing a variable line-of-sight projection of the field vector, often reveals a more complex field structure than a simple dipole (Martin & Wickramasinghe 1984) as found in the cases of the fast-rotating ($P \approx 12$ min) white dwarf J0317–855 (see Burleigh, Jordan, & Schweizer 1999; Vennes et al. 2003) or the “spotted” magnetic white dwarf WD 1953–011 with a rotation period of 1.4 day (Maxted et al. 2000; Brinkworth et al. 2005; Valyavin et al. 2008). Apart from the common hypothesis of a fossil origin, magnetic fields may be generated in later stages as first proposed by Tout et al. (2008), first, during a common-envelope (CE) phase of binary evolution (see also Potter & Tout 2010; Nordhaus et al. 2011) or in a double degenerate merger (see also García-Berro et al. 2012).

Kawka & Vennes (2004) examined the distribution of field strength in the Ap star population and concluded that a direct link between Ap stars and high field magnetic white dwarfs ($B \gtrsim 10^7$ G) may exist assuming magnetic flux conservation, but that low-field white dwarfs are without known progenitors. However, Wickramasinghe & Ferrario (2005) found a progenitor deficit for high-field white dwarfs and

^{*} Based on observations made with ESO telescopes at the La Silla Paranal Observatory under programme IDs 80.D-0521, 82.D-0521, 83.D-0750 and 84.D-0862.

[†] E-mail: kawka@sunstel.asu.cas.cz (AK); vennes@sunstel.asu.cas.cz (SV)

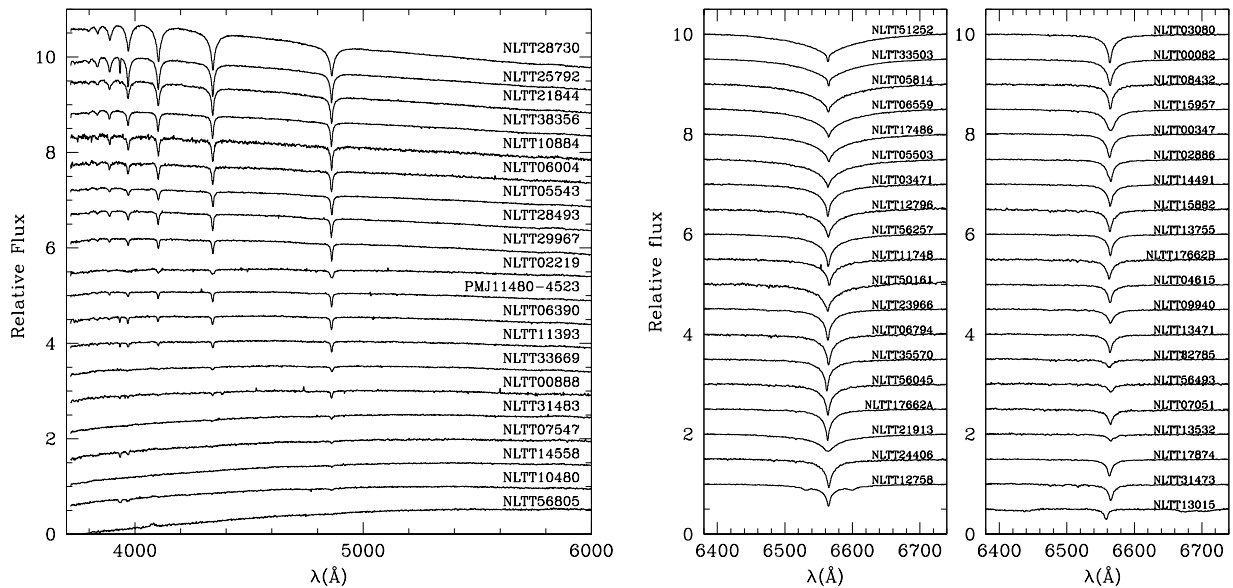


Figure 1. VLT/FORS spectra of DA white dwarfs ordered by increasing temperatures (bottom to top and right to left): 20 spectra were obtained (left panel) using grism 600B and covering the upper Balmer lines, and (right panel) 39 spectra were obtained using grism 1200R+93 and covering H α . Several objects show Ca K (NLTT 888, 6390, 7547, 10480, 11393, and 25792) in their spectra with a few more showing CaI λ 4226 (NLTT 7547, 10480, and 25792) and are classified as DAZ white dwarfs. Zeeman line splitting is immediately apparent in the H α spectra of NLTT 12758 and 13015.

postulated that a large fraction of massive main-sequence stars ($\gtrsim 4.5 M_{\odot}$) may harbour weak fields (10-100 G).

We present a survey of 58 high proper-motion white dwarfs conducted with the FOcal Reducer and low dispersion Spectrograph (FORS) at the European Southern Observatory (ESO). The observations, presented in Section 2, provided us with intensity and circular polarization spectra enabling high-sensitivity measurements of the surface-averaged (B_s) and longitudinal (B_l) magnetic fields (Section 3). In particular, we examine the sample properties (Section 3.1), our new low-field detections (Section 3.2) and instances of variable high-fields (Section 3.3), and the sample kinematical properties (Section 3.4) as well as other interesting aspects of this survey (Section 3.5). We summarize and discuss some implications of our results in Section 4.

2 OBSERVATIONS

We obtained two sets of observations using the FORS spectrograph attached to the 8m telescopes at Paranal Observatory. The first data set was obtained with the FORS1 attached to UT2. We used the 600 lines per mm grism centred at 4650 Å (Grism 600B). The slit width was set to 1.0 arcsec to obtain a spectral dispersion of 1.51 Å per pixel and a resolution of ~ 6 Å. The second set of observations was obtained with the FORS2 attached to UT1. For these observations we used the 1200 lines per mm grism centred at 6500 Å (Grism 1200R+93) providing a spectral dispersion of 0.73 Å per pixel. The slit width was set to 1.0 arcsec to obtain a spectral resolution of 3.0 Å. Both sets of spectra were obtained in the spectropolarimetric mode where the observing sequence consisted of an exposure with the Wol-

laston prism rotated to -45° immediately followed by an exposure with the Wollaston prism rotated to $+45^\circ$.

Additional spectra of the programme stars were obtained at ESO using the New Technology Telescope (NTT) and at Cerro Tololo Inter-American Observatory (CTIO) and Kitt Peak National Observatory (KPNO). We also collected spectra from the Sloan Digital Sky Survey (SDSS) Data Release 8, and recycled our published spectra (Kawka & Vennes 2006). The complete data set will be described in a forthcoming publication and, here, we employ key results of the spectroscopic analysis of these complementary spectra. In summary, the spectra obtained with the NTT have a resolution of ~ 14 Å and a spectral range of 3700 - 7400 Å, the spectra obtained with the CTIO 4m telescope have a resolution of ~ 8 Å with a spectral range of 3700 - 7480 Å, and the spectra obtained with the KPNO 4m telescope have a resolution of ~ 5.5 Å and a spectral range of 3660 - 6790 Å. The SDSS spectra cover a range from 3800 to 9200 Å and have a resolution of ~ 3 Å.

The data were reduced using standard IRAF procedures. The stars observed during P80 (FORS1) were flux calibrated using the standard stars Feige 110, EG 21 and EG 274.

Table 1 lists the selected targets. Figure 1 shows the intensity spectra obtained during the two FORS programmes. Some of the blue spectra showed heavy element lines (Ca H&K) characteristic of polluted DA white dwarfs (DAZ), while the red spectra only showed H α with the exception of the spectrum of NLTT 11748: the strong, saturated Na D doublet ($W(D2) = 220 \pm 20 \text{ mÅ}$, $W(D1) = 210 \pm 20 \text{ mÅ}$) at a heliocentric velocity of $v = 20 \pm 3 \text{ km s}^{-1}$ revealed a high neutral gas (NaI) column density in the interstellar medium (ISM) toward the star. The Na D doublet was not

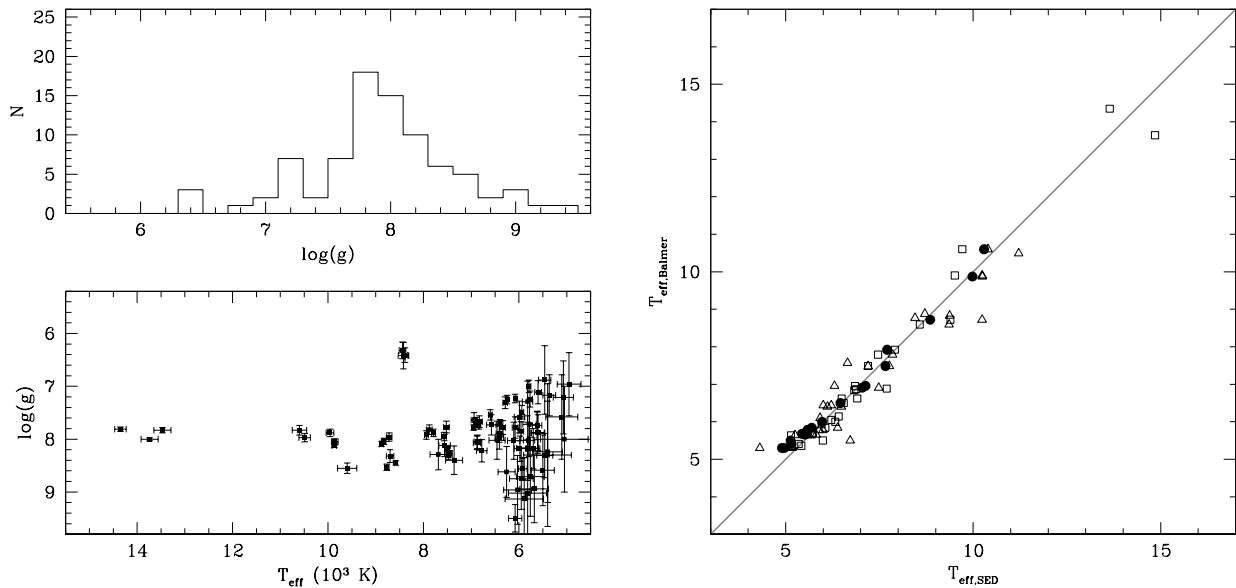


Figure 2. (Bottom left panel) set of 83 surface gravity and effective temperature measurements of the sample of 56 stars that exclude the two high-field DAP white dwarfs. The measurement errors increase with decreasing effective temperature. The low-gravity star near $T_{\text{eff}} = 8500$ K is NLTT 11748. (Top left panel) the distribution of surface gravity measurements shows high- and low-gravity tails that are mostly accounted for by large errors in surface gravity measurements. (Right panel) Adopted effective temperatures versus effective temperatures determined using colours described in Appendix A: SDSS *ugriz* (full circles), $V - J$ (open squares), and $R - J$ (open triangles).

detected toward any other objects from our sample. The star NLTT 11748 is located toward a known high-density line-of-sight (Vergely et al. 2001; Welsh et al. 2010) and the scaled ISM H I column density (10^{21} cm^{-2}) correlates well with the relatively large extinction coefficient $E_{B-V} = 0.1$ measured by Kawka & Vennes (2009).

Observations of the DC white dwarfs NLTT 8525, NLTT 8904, NLTT 11051, NLTT 20389, and PM J04356–6105, of the DZ white dwarfs NLTT 57760 and PM J08186–3110, and of the DQ white dwarfs NLTT 8733 and NLTT 14553 will be presented in a forthcoming publication. Two targets that were subsequently reclassified are not listed: NLTT 18393 (M3.5) and NLTT 40020 (G5V). Finally, we also excluded one observation of NLTT 17486 obtained on UT 2007 October 31 and all observations of NLTT 40636 because of pointing errors. The coordinates and proper-motion measurements are from Salim & Gould (2003).

The circular polarization spectra were obtained using two successive exposures obtained with the Wollaston prism rotated to the angle $\theta = -45^\circ$ and $+45^\circ$ and were calculated following:

$$v = V/I = \frac{1}{2} \left[\left(\frac{f_o - f_e}{f_o + f_e} \right)_{\theta=45^\circ} - \left(\frac{f_o - f_e}{f_o + f_e} \right)_{\theta=-45^\circ} \right] \quad (1)$$

where f_o and f_e are the fluxes from the ordinary and extra-ordinary beams, respectively. The direction of polarization of these beams are perpendicular to each other. This method is used to eliminate possible biases to first order (Bagnulo et al. 2002).

2.1 Imaging and photometry

We calibrated the acquisition images and converted the count rates into broad-band magnitudes. The procedure is described in Appendix A and the magnitudes are listed in Table A1 along with published V magnitudes and Two Micron All Sky Survey (2MASS) J magnitudes. A close examination of the acquisition images of NLTT 17662 revealed the presence of a close (sep. ≈ 1.6 arcsecond, $P.A. = 340^\circ$) companion to the white dwarf approximately 1 mag fainter. A comparison with the first-epoch Digitized Sky Survey (DSS) image proves that the faint companion is in common proper-motion with the bright star. Fortunately, both stars were acquired during the spectroscopic observations and we were able to analyse both FORS spectra. Similarly, our acquisition image of NLTT 56045 also reveal the presence of a close common proper-motion companion 1.1 mag fainter in white light (sep. ≈ 2.2 arcsecond, $P.A. = 290^\circ$). The faint component was also acquired during spectroscopic observations but no spectra were extracted.

Finally, we cross-correlated our sample of stars with the SDSS Data Release 8 and obtained *ugriz* photometry for 18 objects. Only one of these had a SDSS spectrum. Table A2 lists the available *ugriz* photometry. A correction of -0.04 mag was applied to the tabulated u magnitude prior to our analysis (see, e.g., Kleinman et al. 2004).

3 ANALYSIS

The hydrogen-rich white dwarfs were analysed for their effective temperature and surface gravity using a grid of pure-hydrogen LTE plane-parallel models. The grid of models ex-

Table 1. VLT FORS observations.

Name	Alternate Names	RA (2000)	Dec (2000)	V_p^a (mag)	μ ($'' \text{ yr}^{-1}$)	UT Date	N^b
NLTT 82	LP644-30, PHL2595, G158-128	00 04 10.34	-03 40 08.54	16.73	0.237	25 Oct 2009	2
NLTT 347	LP764-69, G158-134	00 08 21.70	-14 35 02.18	16.86	0.169	25 Oct 2009	2
NLTT 888	LHS5002, LP644-81	00 17 37.72	-05 16 46.42	17.82	0.475	15 Nov 2007	1
						12 Dec 2007	1
NLTT 2219	LP645-70, PB8467	00 40 56.18	-08 09 08.82	17.19	0.426	14 Dec 2007	2
NLTT 2886	LP882-92	00 52 08.94	-30 36 39.67	16.48	0.196	15 Oct 2009	2
NLTT 3080	G270-98, EG6, LP706-65	00 55 50.34	-11 27 31.50	15.36	0.439	25 Nov 2009	1
						02 Dec 2009	1
						21 Dec 2009	1
NLTT 3471	PHL3287, G270-123, LP646-83	01 03 19.63	-03 24 59.76	16.60	0.178	25 Oct 2009	1
						26 Oct 2009	1
NLTT 4615	LP587-53	01 23 14.71	-02 09 27.00	17.13	0.246	26 Oct 2009	2
NLTT 5503	G271-117, LP648-27, PHL1086	01 38 52.58	-03 56 50.17	16.43	0.187	02 Dec 2009	1
						03 Dec 2009	1
NLTT 5543	LHS1274, LP939-114	01 39 14.38	-33 49 03.87	17.34	0.595	08 Oct 2007	2
NLTT 5814	GD1394, MCT0142-3026	01 44 36.27	-30 11 22.38	16.22	0.189	15 Oct 2009	1
NLTT 6004	G274-95, LP884-35, HE0145-2726	01 47 43.93	-27 11 36.89	15.84	0.320	03 Nov 2007	1
NLTT 6390	LP884-58	01 54 05.36	-30 34 32.41	17.08	0.489	01 Nov 2007	1
NLTT 6559	LP649-6, KUV01552-0703	01 57 41.91	-06 48 46.87	16.57	0.261	06 Jan 2010	1
						25 Jan 2010	1
NLTT 6794	G274-137, LP884-82	02 01 41.26	-26 50 38.26	16.87	0.255	16 Oct 2009	1
						25 Jan 2010	1
NLTT 7051	LP885-22	02 07 02.33	-30 23 32.42	16.18	0.266	15 Oct 2009	1
NLTT 7547	LP649-83	02 17 19.63	-06 56 28.86	17.89	0.391	13 Dec 2007	2
NLTT 8432	LP830-13	02 35 21.69	-22 51 21.96	17.02	0.278	30 Nov 2009	1
						01 Feb 2010	1
NLTT 9940	LP651-74	03 07 13.91	-07 15 06.23	17.23	0.491	24 Nov 2009	2
NLTT10480	LHS5070, LP887-66	03 17 12.08	-29 11 34.33	17.30	0.496	01 Nov 2007	1
NLTT10884	LP772-61	03 25 15.50	-17 22 27.77	16.46	0.320	27 Oct 2007	1
NLTT11393	LP832-30, WT1384	03 36 34.09	-22 15 24.05	17.21	0.346	03 Nov 2007	1
NLTT11748	LP413-40	03 45 16.83	+17 48 08.71	16.66	0.295	22 Oct 2009	3
						23 Oct 2009	2
NLTT12758	G160-51	04 12 26.33	-11 17 47.33	15.46	0.285	23 Oct 2009	3
						24 Nov 2009	2
NLTT12796	GD58	04 13 38.67	-08 01 28.88	16.37	0.202	03 Dec 2009	1
						15 Jan 2010	1
NLTT13015	LP714-52	04 19 21.10	-09 34 29.57	17.50	0.182	22 Oct 2009	1
						10 Nov 2009	1
						24 Nov 2009	1
NLTT13471	LP775-28	04 32 00.35	-19 20 49.85	16.97	0.263	09 Jan 2010	1
						25 Jan 2010	1
						31 Jan 2010	1
NLTT13532	LP890-39	04 33 33.58	-27 53 24.79	16.68	0.388	16 Oct 2009	1
						25 Jan 2010	1
						01 Feb 2010	1
NLTT13755	LP 775-37	04 41 05.03	-15 19 03.51	16.83	0.183	09 Dec 2009	2
NLTT14491	LP776-52	05 05 32.43	-17 31 37.41	17.13	0.314	24 Jan 2010	2
NLTT14558	LHS1739, LP777-3	05 08 36.36	-15 23 13.06	17.69	0.599	31 Jan 2008	2
NLTT15882	LP659-7	05 59 00.96	-04 14 26.88	17.00	0.245	30 Jan 2010	2
						01 Feb 2010	2
NLTT15957	G105-4	06 02 31.10	+15 53 04.85	16.76	0.315	09 Dec 2009	2
NLTT17486	LHS1898, LP896-18	07 09 25.09	-32 05 07.30	15.87	0.530	15 Oct 2009	1
NLTT17662A/B	G89-10, LTT17958, EG171	07 18 08.64	+12 29 59.24	15.89	0.298	08 Dec 2009	1
NLTT17874	LP428-34	07 27 04.15	+14 34 40.22	16.96	0.195	12 Dec 2009	2
NLTT21844	G49-7, G41-39, LP427-59, SDSS	09 28 40.22	+18 41 14.42	15.92	0.302	01 Mar 2008	1
NLTT21913A/B	EC09273-1719, LP787-49	09 29 43.17	-17 32 50.54	15.93	0.449	09 Dec 2009	1
NLTT23966	LP669-73	10 18 33.18	-04 42 28.58	16.76	0.168	23 Jan 2010	2

^a Photographic magnitudes from Salim & Gould (2003).^b Number of complete spectropolarimetric sequences.

Table 1 – continued

Name	Alternate Names	RA (2000)	Dec (2000)	V_p^a (mag)	μ ($'' \text{ yr}^{-1}$)	UT Date	N^b
NLTT24406	LP430-25, SDSS	10 27 47.79	+19 28 24.53	17.10	0.383	03 Feb 2010	1
						09 Feb 2010	1
						14 Feb 2010	1
NLTT25792	EC10542-2236, LP849-31	10 56 38.63	-22 52 55.96	15.64	0.302	07 Mar 2008	1
NLTT28493	LHS2455, G11-020	11 46 25.78	-01 36 36.76	16.19	0.562	29 Mar 2008	1
NLTT28730	LP673-41	11 50 33.33	-06 36 17.06	16.56	0.323	28 Mar 2008	1
						30 Mar 2008	1
NLTT29967	LP674-29	12 12 36.02	-06 22 18.12	17.26	0.443	30 Mar 2008	1
NLTT31473	LHS339, LP853-15	12 40 24.15	-23 17 43.80	16.68	1.114	31 Jan 2010	1
						01 Feb 2010	1
						09 Feb 2010	1
						05 Mar 2010	1
						06 Mar 2010	1
NLTT31483	LHS2601, LP435-447	12 40 30.51	+18 07 28.96	17.42	0.595	31 Mar 2008	2
NLTT32785	LP676-58	13 04 46.39	-05 28 37.74	17.12	0.278	31 Jan 2010	1
						05 Mar 2010	1
						07 Mar 2010	1
NLTT33503	LP737-47, LHS271	13 16 43.60	-15 35 58.45	15.07	0.710	05 Mar 2010	1
NLTT33669	LP854-50, WT2034	13 19 24.76	-21 47 54.85	16.35	0.455	09 Mar 2008	1
NLTT35570	LP912-27	13 53 47.16	-27 38 54.24	16.75	0.198	05 Mar 2010	2
NLTT38356	LP914-20	14 47 22.33	-30 35 23.89	17.44	0.323	31 Mar 2008	2
NLTT50161	LP928-33	20 56 08.33	-27 17 23.64	17.19	0.171	29 Nov 2009	1
NLTT51252	LP873-45, EG502	21 26 26.30	-22 43 53.33	15.59	0.207	28 Nov 2009	1
NLTT56045A/B	LP933-63	23 10 46.39	-29 48 30.64	16.52	0.271	21 Dec 2009	1
NLTT56257	LP822-40	23 15 30.40	-14 40 05.81	15.13	0.186	30 Nov 2009	1
						16 Dec 2009	1
NLTT56493	LP702-67	23 19 35.43	-02 29 00.96	16.89	0.238	16 Dec 2009	1
NLTT56805	LP522-46	23 25 19.86	+14 03 39.42	15.81	0.353	27 Oct 2007	1
PMJ11480-4523	WD1145-451	11 48 03.32	-45 23 01.8	15.66	0.635	07 Mar 2008	1

^a Photographic magnitudes from Salim & Gould (2003), except PMJ11480-4523 from Lépine (2005).

^b Number of complete spectropolarimetric sequences.

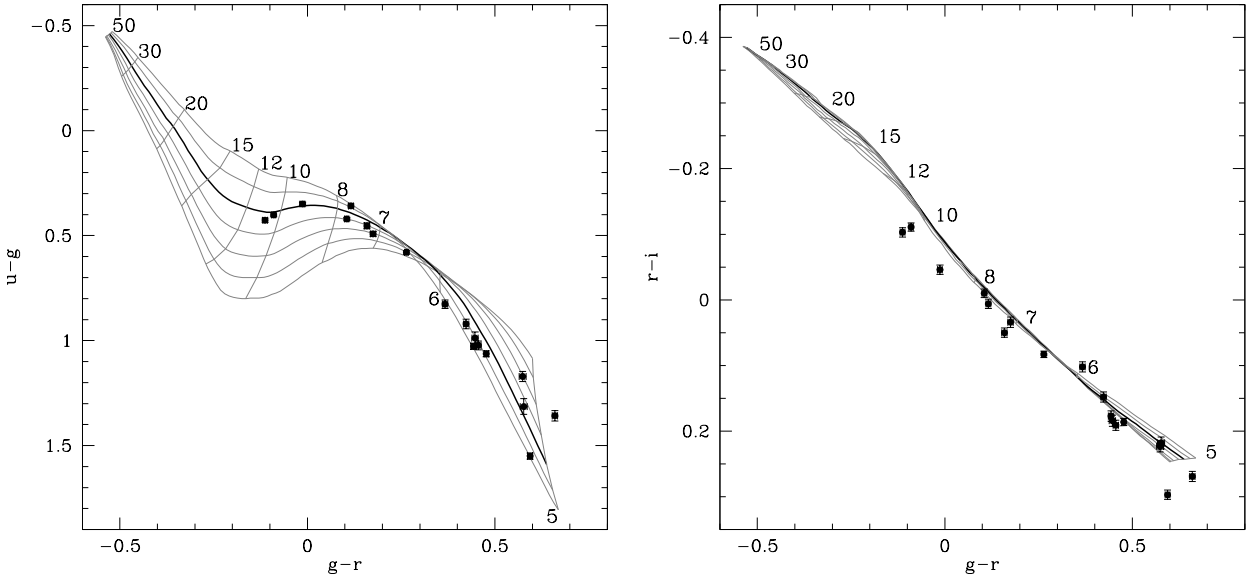


Figure 3. SDSS $u-g$ versus $g-r$ (left panel) and $g-r$ versus $r-i$ (right panel) photometry compared to synthetic colours of H-rich white dwarfs. The effective temperature is indicated in units of 1000 K and $\log g = 6.0$ to 9.0 (in steps of 0.5 from bottom to top). The thick line indicates $\log g = 8$.

tends from $T_{\text{eff}} = 4900$ K to 8000 K (in steps of 100 K), from 8200 to 10000 K (in steps of 200 K) and from 10500 to 20000 K (in steps of 500 K) at $\log g = 5.5$ to 9.5 (in steps of 0.25 dex). The models are described in Kawka & Vennes (2006) and Kawka et al. (2007) with some upgrades described in Kawka & Vennes (2012). The observed Balmer line profiles were fitted with model spectra using χ^2 minimization techniques. The quoted uncertainties are only statistical (1σ) and do not take into account possible systematic effects in model calculations, data acquisition or reduction procedures.

We used the evolutionary mass-radius relations of Benvenuto & Althaus (1999) to convert the measured effective temperature and surface gravity measurements into white dwarf ages and masses. For hydrogen-rich white dwarfs we used the models with $M_H/M_* = 10^{-4}$ and a metallicity of $Z=0$. For helium rich white dwarfs, we used the models of Benvenuto & Althaus (1999) without a hydrogen envelope. The evolutionary tracks of Serenelli et al. (2002) were employed to interpret the parameters of the extremely low-mass white dwarf NLTT 11748.

The longitudinal magnetic field was determined by first fitting the Balmer line profiles with a model profile. We then used this best-fitting model profile to calculate the V/I spectra at various magnetic field strengths (B_1 in Gauss):

$$V/I = \frac{B_1 4.67 \times 10^{-13} \lambda^2 dF}{F d\lambda}, \quad (2)$$

in first order, where λ is the wavelength in \AA and F is the spectral flux. This grid of synthetic circular polarization spectra are then fitted to the observed circular polarization spectra using χ^2 minimization techniques.

The procedure applied to our flux calibration standards EG 21 (WD 0310–688) and EG 274 (WD 1620–391) provided field measurements of $B_1 = -8.1 \pm 6.2$ and 0.5 ± 3.5 kG, respectively, using the $H\beta$, γ , and δ lines. The errors are comparable to other measurements from this programme owing to the relatively short exposure times employed when observing standards. The present results confirm the null results obtained by Kawka et al. (2007) who measured $B_1 = -6.1 \pm 2.2$ (EG 21) and -3.0 ± 2.6 kG (EG 274) using the $H\alpha$, β , and γ lines.

3.1 Sample properties

3.1.1 T_{eff} and $\log g$ measurements

Table 2 lists the measured atmospheric parameters of the sample stars. Using Balmer lines alone, the errors in surface gravity measurements increase considerably at low temperatures $T_{\text{eff}} \lesssim 6500$ K. Figure 2 (left panels) shows the gravity versus temperature measurements based on fitting of the Balmer lines. The data set, which excludes the high-field DAP white dwarfs NLTT 12758 and 13015, comprises 83 individual measurements obtained using different instruments described in Section 2. The surface gravity distribution, excluding NLTT 11748, is consistent with a sample average $\langle \log g \rangle = 7.92$ and an intrinsic width $\sigma = 0.36$ dex ($\chi^2 = 1$) corresponding to an average mass of $0.54^{+0.23}_{-0.15} M_{\odot}$. The average mass is lower than determined for younger white dwarf samples such as the SDSS white dwarf sample for which mean masses of $0.593 M_{\odot}$ (Kepler et al.

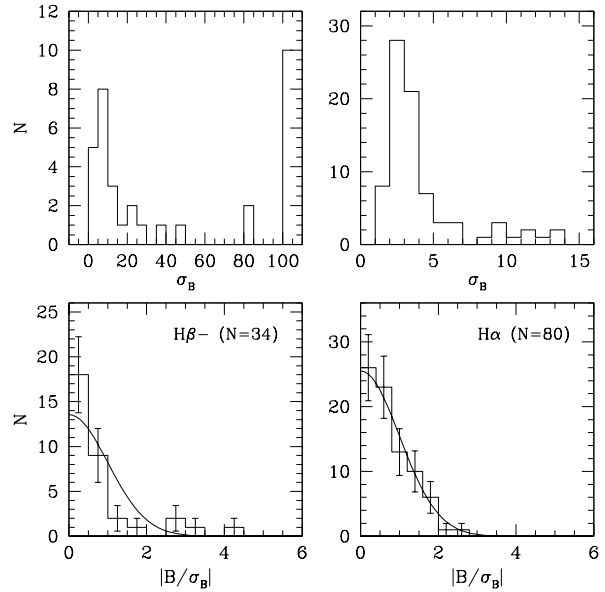


Figure 4. Error statistics of the magnetic field measurements: (upper panels) error distributions in the longitudinal field strength when measuring the upper Balmer lines (left panels) or $H\alpha$ (right panels), and (lower panels) the corresponding distributions of the measurement significance (B/σ_B). We obtained 34 individual measurements of the upper Balmer lines and 80 individual measurements of $H\alpha$ for 20 and 39 stars, respectively.

2007) and $0.613 M_{\odot}$ (Tremblay et al. 2011) were determined. Gianninas, Bergeron, & Ruiz (2011) determined a mean mass of $0.661 M_{\odot}$ from their spectroscopic analysis of white dwarfs selected from the McCook & Sion catalogue (McCook & Sion 1999). Recently, Giammichele et al. (2012) reanalysed the local sample of white dwarfs and determined a mean mass of $0.650 M_{\odot}$.

Figure 3 shows photometric data of a sub-sample of 18 of these objects and synthetic colours computed using our model atmosphere grid. The observed colours clearly show the effect of extended $\text{Ly}\alpha$ absorption described by Kowalski & Saumon (2006).

Several measurements based on Balmer lines, particularly those excluding $H\alpha$, are unsatisfactory below ~ 6500 K. In such cases where the error on the surface gravity exceeded 0.5 dex, we adopted the average and dispersion of gravity measurements for stars with temperatures above ~ 6500 K, i.e., $\langle \log g \rangle = 8.0$ and $\sigma_g = 0.24$, and we fitted the Balmer lines within this constraint to determine the temperature. Next, we compared the adopted effective temperatures to measurements based on SDSS *ugriz* photometry and on the $V - J$ and $R - J$ indices: Figure 2 (right panel) show the measurements obtained using the various methods. The results based on Balmer lines and the $V - J$ index differ by 16 K only with a dispersion of 412 K. Those based on the $R - J$ index differ from the Balmer line results by 72 K with a dispersion of 552 K. The temperatures measured using the SDSS *ugriz* data differ by -117 K on average but with a lower dispersion of 189 K. The latter also suggest that the effective temperature of cool white dwarfs ($\lesssim 5500$ K) ob-

Table 2. Atmospheric and other properties.

WD	NLTT	Adopted parameters ^a					
		T_{eff} (K)	$\log g$ (c.g.s)	Mass (M_{\odot})	Age (Gyr)	M_V (mag)	d (pc)
0001–039	00082	6910 ± 40	7.67 ± 0.08	0.43 ± 0.03	1.5	13.15 ± 0.09	53 ± 2
0005–148 ^b	00347	6400 ± 180	(8.00 ± 0.24)	0.59 ± 0.15	2.0	13.95 ± 0.42	42 ± 8
0015–055 ^c	00888	5680 ± 190	(8.00 ± 0.24)	0.59 ± 0.15	2.9	14.49 ± 0.47	43 ± 9
0038–084 ^d	02219	6000 ± 180	(8.00 ± 0.24)	0.59 ± 0.15	2.4	14.23 ± 0.44	41 ± 8
0049–308	02886	6440 ± 180	(8.00 ± 0.24)	0.59 ± 0.15	2.0	13.92 ± 0.42	55 ± 6
0053–117	03080	6840 ± 40	7.72 ± 0.09	0.44 ± 0.04	1.3	13.28 ± 0.13	25 ± 2
0100–036	03471	8720 ± 60	7.96 ± 0.08	0.57 ± 0.05	0.84	12.66 ± 0.12	61 ± 3
0120–024 ^e	04615	5840 ± 210	(8.00 ± 0.24)	0.59 ± 0.15	2.6	14.35 ± 0.47	42 ± 9
0136–042	05503	9870 ± 50	8.12 ± 0.04	0.67 ± 0.02	0.78	12.43 ± 0.06	60 ± 2
0136–340	05543	6620 ± 160	(8.00 ± 0.24)	0.59 ± 0.15	1.8	13.80 ± 0.40	47 ± 9
0142–304	05814	10490 ± 120	7.97 ± 0.08	0.58 ± 0.05	0.53	11.98 ± 0.13	79 ± 5
0145–274	06004	6620 ± 230	(8.00 ± 0.24)	0.59 ± 0.15	1.8	13.80 ± 0.45	32 ± 7
0151–308 ^c	06390	6050 ± 180	(8.00 ± 0.24)	0.59 ± 0.15	2.4	14.19 ± 0.44	42 ± 8
0155–070	06559	10600 ± 150	7.83 ± 0.09	0.51 ± 0.05	0.42	11.75 ± 0.16	84 ± 6
0159–270	06794	7480 ± 50	8.30 ± 0.08	0.78 ± 0.05	2.3	13.77 ± 0.10	49 ± 2
0204–306 ^e	07051	5640 ± 200	(8.00 ± 0.24)	0.58 ± 0.15	2.9	14.52 ± 0.48	30 ± 7
0214–071 ^c	07547	5410 ± 200	(8.00 ± 0.24)	0.58 ± 0.15	3.4	14.73 ± 0.50	44 ± 10
0233–230	08432	6440 ± 200	(8.00 ± 0.24)	0.59 ± 0.15	2.0	13.92 ± 0.43	45 ± 9
0304–074	09940	5660 ± 270	(8.00 ± 0.24)	0.58 ± 0.15	2.9	15.50 ± 0.46	37 ± 9
0315–293 ^f	10480	5340 ± 190	(8.00 ± 0.24)	0.58 ± 0.15	3.7	14.79 ± 0.49	33 ± 8
0322–175	10884	6884 ± 42	7.66 ± 0.09	0.42 ± 0.03	1.6	13.15 ± 0.10	64 ± 3
0334–224 ^c	11393	5930 ± 170	(8.00 ± 0.24)	0.59 ± 0.15	2.5	14.28 ± 0.43	36 ± 7
0342+176	11748	8412 ± 42	6.38 ± 0.10	0.17 ± 0.01	4.5	10.11 ± 0.07	204 ± 7
0410–114 ^d	12758	7440 ± 150	(8.00 ± 0.24)	0.59 ± 0.15	1.3	13.34 ± 0.38	26 ± 5
0411–081	12796	8830 ± 40	8.04 ± 0.06	0.62 ± 0.04	0.92	12.73 ± 0.09	51 ± 2
0416–096 ^d	13015	5745 ± 405	(8.00 ± 0.24)	0.59 ± 0.15	2.8	14.43 ± 0.66	40 ± 12
0429–194	13471	5780 ± 210	(8.00 ± 0.24)	0.59 ± 0.15	2.7	14.40 ± 0.48	34 ± 7
0431–279	13532	5300 ± 220	(8.00 ± 0.24)	0.58 ± 0.15	3.8	14.83 ± 0.53	24 ± 6
0438–154	13755	6000 ± 160	(8.00 ± 0.24)	0.59 ± 0.15	2.4	14.23 ± 0.42	33 ± 8
0503–175	14491	6140 ± 180	(8.00 ± 0.24)	0.59 ± 0.15	2.3	14.13 ± 0.43	41 ± 8
0506–154	14558	5360 ± 210	(8.00 ± 0.24)	0.58 ± 0.15	3.6	14.78 ± 0.51	39 ± 9
0556–042	15882	6100 ± 190	(8.00 ± 0.24)	0.59 ± 0.15	2.3	14.16 ± 0.44	40 ± 8
0559+158	15957	6870 ± 70	8.05 ± 0.13	0.62 ± 0.08	1.8	13.72 ± 0.19	41 ± 4
0707–320	17486	9903 ± 52	7.98 ± 0.05	0.59 ± 0.03	0.62	12.20 ± 0.08	48 ± 2
0715+125A	17662A	7560 ± 120	8.12 ± 0.21	0.67 ± 0.14	1.6	13.45 ± 0.30	33 ± 4
0715+125B	17662B	6025 ± 75	8.25 ± 0.25	0.75 ± 0.16	3.6	14.58 ± 0.30	...
0724+146	17874	5780 ± 240	(8.00 ± 0.24)	0.59 ± 0.15	2.7	14.40 ± 0.50	31 ± 7
0925+189	21844	7487 ± 30	8.22 ± 0.04	0.73 ± 0.03	2.0	13.64 ± 0.05	40 ± 1
0927–173A ^g	21913	9550 ± 115	8.58 ± 0.07	0.96 ± 0.04	1.8	13.31 ± 0.10	43 ± 2
1016–044	23966	7790 ± 40	7.88 ± 0.07	0.52 ± 0.04	0.99	12.99 ± 0.10	67 ± 4
1025+197	24406	6959 ± 73	8.13 ± 0.12	0.67 ± 0.08	2.0	13.79 ± 0.17	51 ± 4
1054–226 ^c	25792	7921 ± 33	7.88 ± 0.06	0.52 ± 0.03	0.95	12.92 ± 0.09	41 ± 2
1143–013	28493	6500 ± 220	(8.00 ± 0.24)	0.59 ± 0.15	1.9	13.88 ± 0.44	32 ± 7
1150–066	28730	8595 ± 28	8.44 ± 0.04	0.87 ± 0.03	2.0	13.47 ± 0.05	41 ± 1
1209–060 ^e	29967	6400 ± 170	(8.00 ± 0.24)	0.59 ± 0.15	2.0	13.95 ± 0.41	41 ± 8
1237–230	31473	5680 ± 150	(8.00 ± 0.24)	0.59 ± 0.15	2.9	14.49 ± 0.43	26 ± 5
1238+183	31483	5500 ± 240	(8.00 ± 0.24)	0.58 ± 0.15	3.2	14.65 ± 0.53	39 ± 10
1302–052	32785	5340 ± 140	(8.00 ± 0.24)	0.58 ± 0.15	3.7	14.79 ± 0.44	30 ± 6
1314–153	33503	14350 ± 120	7.81 ± 0.04	0.51 ± 0.02	0.17	11.04 ± 0.06	58 ± 2
1316–215	33669	5690 ± 150	(8.00 ± 0.24)	0.59 ± 0.15	2.8	14.48 ± 0.43	28 ± 6
1350–274	35570	7570 ± 50	7.95 ± 0.08	0.56 ± 0.05	1.2	13.20 ± 0.12	56 ± 3
1444–303	38356	6950 ± 30	7.78 ± 0.05	0.47 ± 0.03	1.2	13.31 ± 0.08	63 ± 2
2053–274	50161	8880 ± 40	8.09 ± 0.05	0.65 ± 0.03	0.98	12.78 ± 0.07	74 ± 3

^a Based on the analysis of Balmer line profiles except for the high-field DAP white dwarfs NLTT 12758 and 13015 (see text).^b Possible DAP white dwarf.^c DAZ white dwarf.^d DAP white dwarf.^e In a common proper-motion binary with a main-sequence star.^f Magnetic DAZ (DAZP) white dwarf (Kawka & Vennes 2011).^g DA+DC binary: (DC) $T_{\text{eff}} = 6150 \pm 150$ K, $\log g = 8.11 \pm 0.12$, $M = 0.63 \pm 0.08 M_{\odot}$.

Table 2 – *continued*

WD	NLTT	Adopted parameters ^a					
		T_{eff} (K)	$\log g$ (c.g.s)	Mass (M_{\odot})	Age (Gyr)	M_V (mag)	d (pc)
2123–229	51252	13605 ± 127	7.95 ± 0.03	0.58 ± 0.02	0.25	11.35 ± 0.05	60 ± 2
2308–300A	56045	7520 ± 60	7.77 ± 0.11	0.47 ± 0.06	0.94	12.98 ± 0.17	57 ± 5
2312–149	56257	8770 ± 50	8.53 ± 0.06	0.93 ± 0.04	2.1	13.56 ± 0.07	26 ± 1
2317–027	56493	5300 ± 220	(8.00 ± 0.24)	0.58 ± 0.15	3.8	14.83 ± 0.53	34 ± 8
2322+137	56805	5300 ± 140	(8.00 ± 0.24)	0.58 ± 0.15	3.8	14.83 ± 0.44	17 ± 4
1145–451	...	6100 ± 150	(8.00 ± 0.24)	0.59 ± 0.15	2.3	14.16 ± 0.41	20 ± 4

^a Based on the analysis of Balmer line profiles.

Table 3. Magnetic field measurements - detections.

NLTT	B_1 (kG)	B_S (kG)	lines
347	-4.2 ± 2.8		H α
	-5.2 ± 2.8		H α
	-4.6 ± 1.9	...	H α
2219	-112.8 ± 38.8		H β , H γ , H δ
	-79.8 ± 26.6		H β , H γ , H δ
	-97.0 ± 21.6	~ 300 .	H β , H γ , H δ
10480 ^a	-212.0 ± 50.0	519 ± 4 .	Ca H&K
12758	...	$(1.7 \pm 0.2) \times 10^3$	H α
13015	...	$(6.0 - 7.5) \times 10^3$	H α

^a From Kawka & Vennes (2011).

tained by fitting Balmer lines assuming $\log g = 8$ may be overestimated by a few 100 K.

Table 2 also lists the absolute magnitude, age, mass, and distance estimates. The distances were obtained by calculating the distance modulus $m - M$ from the absolute and apparent magnitudes (Appendix A). The DA white dwarfs NLTT 3080, NLTT 13532, NLTT 56805, and PM J11480–4523 probably reside within 25 pc from the Sun.

3.1.2 Magnetic field measurements

Probable or definite non-zero field measurements are reported in Table 3 where bold-faced entries are weighted averages, and Table 4 lists average field measurements that are statistically consistent with the null hypothesis. The uncertainties vary and are lower when measuring strong, narrow lines. For example, the error obtained in measuring the Ca H&K lines in NLTT 7547 is a factor of four lower than obtained in measuring the shallow Balmer lines.

Figure 4 shows the error distributions obtained using the H α or the upper-Balmer set-ups. The sample depicted in the diagram excludes the strong-field objects NLTT 12758 and NLTT 13015. The errors are typically of the order of 2–3 kG when measuring H α , and the errors increase to 5–10 kG when measuring the upper Balmer lines. The field distribution obtained using the upper Balmer lines also shows a systematic offset of 4 kG. The significance of the measurements, B/σ_B , closely follows a normalized Gaussian distribution when measuring H α , but the distribution obtained

when measuring the less significant upper Balmer lines departs somewhat from expectations indicating that the errors were overestimated by $\lesssim 50\%$. Two outliers stood out, NLTT 2219 in the upper-Balmer distribution and NLTT 347 in the H α distribution.

3.2 New low-field magnetic white dwarfs

NLTT 347 is most likely a new weak-field magnetic white dwarf. We measured a longitudinal field of -4.6 ± 1.9 kG field in the co-added spectrum, which is a 2.4σ detection. Figure 5 (left) shows the combined flux and circular polarization spectra of H α compared to the best fit models. For individual measurements we obtained a similar field-strength although at a lower significance.

NLTT 2219 is a cool magnetic white dwarf. Figure 5 (right) shows the flux and polarization spectra. The flux spectrum shows a rounded core due to the weak magnetic field, and the circular polarization spectrum clearly shows the effect of a weak magnetic field.

We reported previously on NLTT 10480 as a new magnetic ($B_S = 519 \pm 4$ kG) DAZ white dwarf (Kawka & Vennes 2011). The polarization and flux spectra of Ca H&K constrained $B_1 = -212 \pm 50$ kG (Kawka & Vennes 2012) suggesting a field inclination of $\approx 60^\circ$. This object is one of the coolest white dwarfs showing heavy element lines.

3.3 New, variable, high-field white dwarfs

NLTT 12758 is a new magnetic white dwarf (Fig. 6). We estimated a temperature of $T_{\text{eff}} = 7440 \pm 150$ K using the $V - J$ index assuming a gravity $\log g = 8$. The Zeeman splitting corresponds to a surface magnetic field of 1.7 ± 0.2 MG. Available photometry ($V = 15.46$, $U - B = -0.71$, $B - V = +0.31$) from Eggen (1968) suggests an effective temperature of ≈ 7700 K, which is in agreement with our determination. The structure of the H α profile of NLTT 12758 appears to be similar to that of the magnetic white dwarf NLTT 48454 (WD 1953–011). Maxted et al. (2000) found that the magnetic field strength of NLTT 48454 varied as shown by variable Zeeman line splitting in the H α core. They proposed a two-component model for the magnetic field structure of the white dwarf, whereby the star has a weak dipolar magnetic field of ~ 70 kG with a much stronger spot-like field of ~ 500 kG. Moreover, as in the case of NLTT 48454, the π component is too strong for

Table 4. Magnetic field measurements - non-detections ($N = 54$).

NLTT	B_1 (kG)	lines	NLTT	B_1 (kG)	lines
82	0.6 ± 1.6	H α	15957	-0.8 ± 1.6	H α
888	-3.9 ± 39.8	H β ,H γ ,H δ	17486	0.4 ± 3.1	H α
2886	-1.5 ± 1.9	H α	17662A	-3.2 ± 2.0	H α
3080	-0.7 ± 1.2	H α	17662B	-3.5 ± 4.7	H α
3471	0.2 ± 2.1	H α	17874	4.6 ± 2.3	H α
4615	-0.3 ± 2.4	H α	21844	0.7 ± 4.8	H β ,H γ ,H δ
5503	2.0 ± 2.5	H α	21913	-1.6 ± 2.2	H α
5543	0.0 ± 5.2	H β ,H γ ,H δ	23966	-3.4 ± 2.2	H α
5814	-0.3 ± 5.0	H α	24406	3.0 ± 2.4	H α
6004	6.8 ± 9.4	H β ,H γ ,H δ	25792	3.9 ± 3.0	H β ,H γ ,H δ
6390	-3.9 ± 10.8	H β ,H γ ,H δ	28493	20.6 ± 7.4	H β ,H γ ,H δ
6559	-3.2 ± 2.2	H α	28730	-2.4 ± 2.0	H β ,H γ ,H δ
6794	-3.2 ± 2.0	H α	29967	-3.6 ± 6.5	H β ,H γ ,H δ
7051	-1.2 ± 6.4	H α	31473	1.0 ± 1.8	H α
7547	-23.5 ± 177.0	H β ,H γ	31483	-2.6 ± 80.5	H β ,H γ
	-32.2 ± 40.2	Ca H&K	32785	9.2 ± 6.3	H α
8432	-0.4 ± 2.2	H α	33503	1.6 ± 1.8	H α
9940	4.0 ± 4.5	H α	33669	-2.8 ± 24.8	H β ,H γ ,H δ
10884	-1.3 ± 12.2	H β ,H γ ,H δ	35570	-3.7 ± 2.9	H α
11393	7.8 ± 15.8	H β ,H γ ,H δ	38356	-4.4 ± 4.1	H β ,H γ ,H δ
11748	-2.6 ± 2.7	H α	50161	-4.1 ± 5.7	H α
12796	-2.3 ± 2.2	H α	51252	-0.3 ± 2.5	H α
13471	-0.1 ± 2.1	H α	56045	2.8 ± 3.4	H α
13532	-5.2 ± 6.3	H α	56257	-2.3 ± 1.7	H α
13755	0.8 ± 1.4	H α	56493	-1.9 ± 13.4	H α
14491	0.4 ± 1.7	H α	56805	-333.9 ± 616.4	H β
14558	7.5 ± 108.0	H β	PMJ11480–4523	0.4 ± 10.5	H β ,H γ ,H δ
15882	2.3 ± 1.5	H α			

the σ components suggesting the simultaneous presence of high- and low- field structures, or that NLTT 12758 is in fact a double degenerate star. Variations in the radial velocity measured using the π component also suggest the presence of a close companion (see Section 3.4). A few resolved magnetic plus non-magnetic double degenerates are known (see, e.g., Girven et al. 2010; Dobbie et al. 2012), while some are, to date, unresolved (e.g., EUVE J1439+75.0 Vennes, Ferrario, & Wickramasinghe 1999; Schmidt et al. 2003). NLTT 12758 may be the first known close double degenerate with a magnetic component.

NLTT 13015 is also a new magnetic DA white dwarf (Fig. 6) with a temperature of 5745 ± 405 (assuming $\log g = 8$) determined using the $V - J$ and $R - J$ indices. We measured a spread in surface magnetic field strength ranging from 6.0 to 7.5 MG. The field is possibly time variable and quadratic Zeeman effects are apparent in π and σ components.

3.4 Radial velocities and kinematics

The H α intensity spectra were well suited for a survey of radial velocity (v_r) variability, and all FORS spectra were used in a detailed kinematical study of this sample of high proper-motion white dwarfs. We measured v_r by fitting a Gaussian function to the narrow H α or H β line cores, or, when available, the Ca H&K lines. The errors were estimated by varying the flux continuum placement. The average and dispersion of the H α velocity measurements are $\bar{v} = 59.3$

and $\sigma_v = 35.3 \text{ km s}^{-1}$, while for the H β /Ca H&K lines they are $\bar{v} = 50.1$ and $\sigma_v = 43.6 \text{ km s}^{-1}$. Individual H α velocity measurements are listed in Appendix B. Radial velocities for NLTT 11748 are listed in Kawka, Vennes, & Vaccaro (2010).

We tested the null hypothesis, i.e., a constant velocity, by plotting the distribution of velocity measurements relative to the mean for each star, $(v_i - \bar{v})/\sigma_v$, where \bar{v} is the weighted average of the individual measurements v_i . The distribution is then compared to a normalized Gaussian function and outliers are identified. First, we noted that the distribution was too broad and that systematic errors, i.e., instrumental artefacts, probably dominated statistical errors when measuring H α velocities and to a lesser extent when measuring the less-accurate upper Balmer lines. Therefore, we added a 5 km s^{-1} systematic error in quadrature, $\sigma_v^2 + (5 \text{ km s}^{-1})^2$, and recovered a normal distribution. Similarly, a normal distribution is recovered for the H β /Ca H&K measurements by adding 10 km s^{-1} in quadrature. Apart from the close double degenerate NLTT 11748 (see Kawka, Vennes, & Vaccaro 2010) and the peculiar DAP NLTT 12758 mentioned above (Section 3.3), two other objects stood out ($\chi^2 > 3$) in this survey as possible close binaries, NLTT 6559 and NLTT 31473. However, many sequences cover only a short time interval ($\lesssim 1 \text{ hr}$) and other likely candidates may emerge (e.g., NLTT 21813, see below).

A comparison with published velocity measurements demonstrates the reliability of the H α velocity scale. Zuckerman et al. (2003) listed a velocity of 27.9 km s^{-1} for NLTT 3080 close to our own measurement of

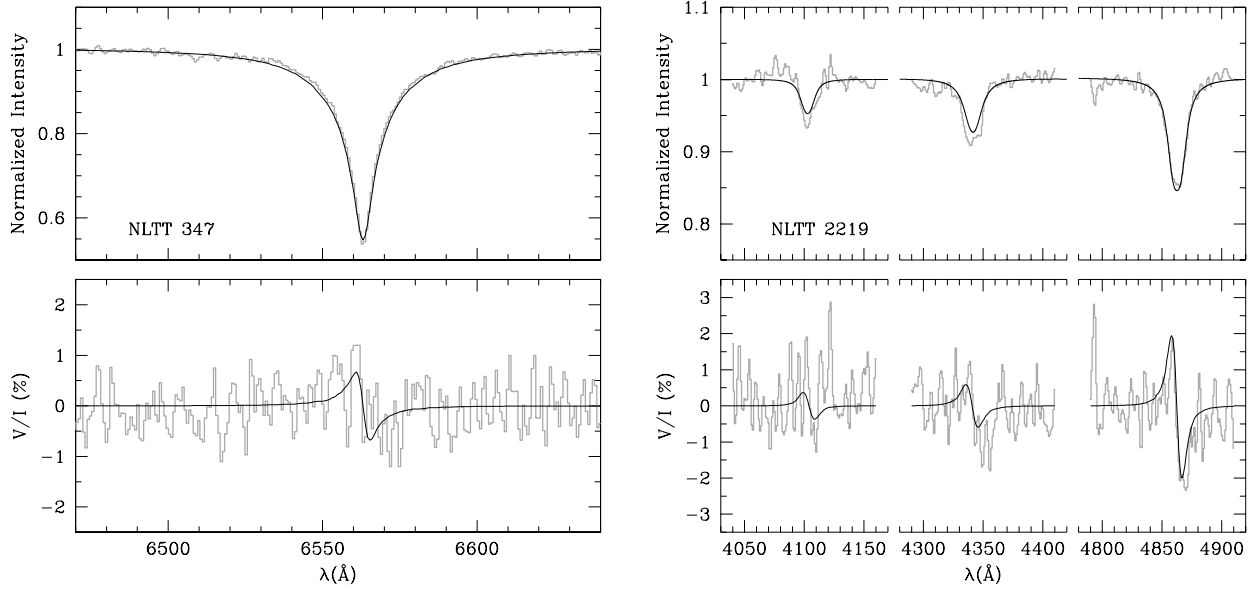


Figure 5. Flux (top left) and circular polarization (bottom left) spectra of NLTT 347. The flux spectrum (grey) is compared to the best fit line profile (black). The circular polarization spectrum (grey) is compared to a model polarization spectrum (black) at $B_1 = -4.6$ kG. Flux (top right) and circular polarization (bottom right) spectra of NLTT 2219. The circular polarization spectra are compared to model polarization spectra at $B_1 = -97$ kG.

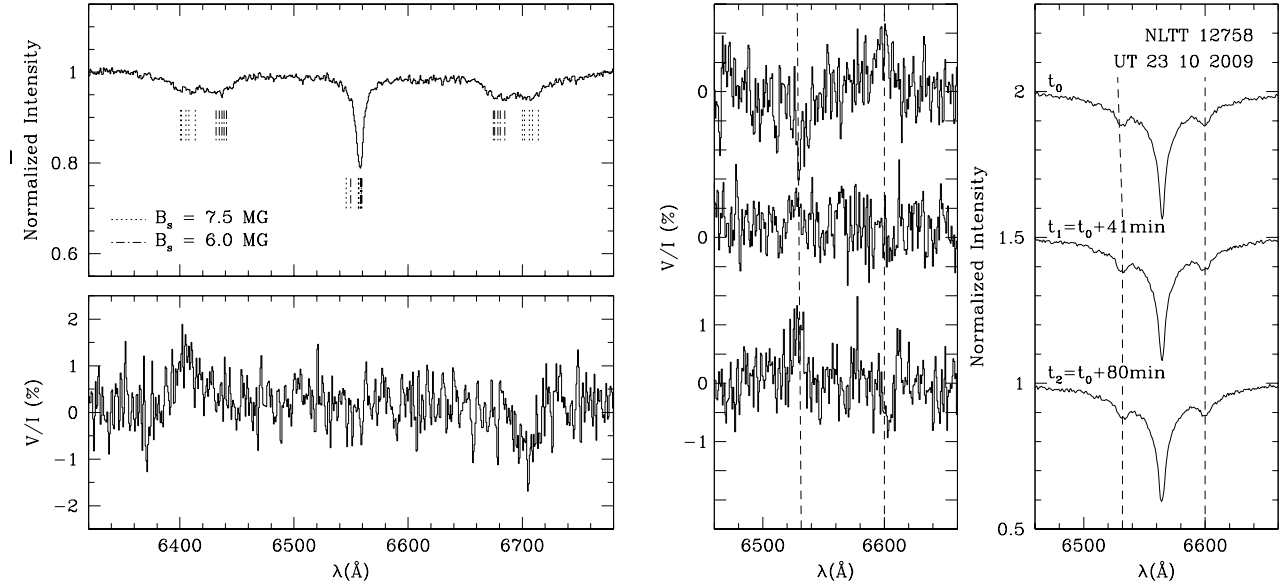


Figure 6. (Upper and lower left panels) intensity and circular polarization (V/I) spectra of the magnetic DA white dwarf NLTT 13015. The intensity spectrum shows a field spread of $\sim 6 - 7.5$ MG and relevant line positions from Kemic (1974) are marked. Intensity (right panel) and circular polarization spectrum (middle panel) of the magnetic DA white dwarf NLTT 12758 showing changes in field orientation within ~ 80 minutes.

28.6 km s^{-1} . The standard deviation of the six measurements (5.1 km s^{-1}), is larger than individual errors ($\sim 1 \text{ km s}^{-1}$), and is probably typical of the limited stability of the FORS velocity scale. Salim et al. (2004) measured a radial velocity $v_r = 74 \pm 7 \text{ km s}^{-1}$ for the candidate halo star NLTT 9940 in agreement with our velocity of $80.5 \pm 3.5 \text{ km s}^{-1}$ (standard

deviation 7.6 km s^{-1}). Maxted & Marsh (1999) measured a radial velocity $v_r = 108.8 \pm 0.8 \text{ km s}^{-1}$ for NLTT 33503 with a low probability of being variable. We measured $111.5 \pm 3.7 \text{ km s}^{-1}$ (measurement and systematic errors added as above) revealing only a small systematic difference. Finally, Kawka & Vennes (2012) measured the radial velocity

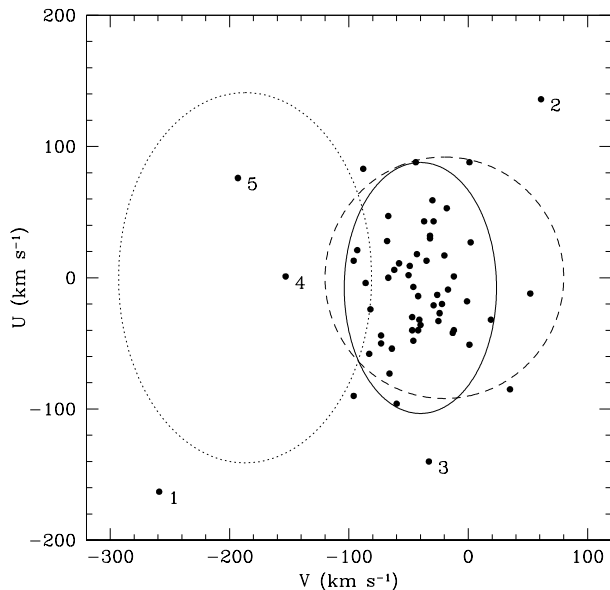


Figure 7. The U and V velocities and 2σ locus (full line) of the NLTT white dwarfs compared to the 2σ thick-disc (dashed line) and 1σ halo ellipses (dotted line) from Chiba & Beers (2000). Stars of interest are marked: (1) NLTT 11748, (2) NLTT 13015, (3) NLTT 17486, (4) NLTT 31473, and (5) NLTT 33503.

of NLTT 23966 with the X-shooter spectrograph and obtained $v_r = 66.4 \pm 5.0 \text{ km s}^{-1}$ in agreement with the present FORS measurement of $58.4 \pm 2.7 \text{ km s}^{-1}$ (standard deviation 7.1 km s^{-1}). On average, our measurements differ by only $\sim 4 \text{ km s}^{-1}$ from published measurements. The differences are comparable to systematic errors of $\sim 5 \text{ km s}^{-1}$.

Similarly, Salim et al. (2004) measured $v_r = 81 \pm 7 \text{ km s}^{-1}$ for NLTT 5543 while we measured $90.3 \pm 5.3 \text{ km s}^{-1}$ using the $H\beta$ line showing similar accuracy.

Figure 7 shows the kinematical properties of our sample in the U versus V Galactic velocity components. We calculated the velocities following Johnson & Soderblom (1987). The effect of the gravitational redshift was removed from the radial velocity measurements. The UVW velocity distributions excluding five peculiar objects (see Fig. 7) follow expected averages and standard deviations of an old population: $(\bar{U}, \bar{V}, \bar{W}) = (-7.8, -40.1, -5.9) \text{ km s}^{-1}$, and $(\sigma_U, \sigma_V, \sigma_W) = (42.8, 31.9, 27.4) \text{ km s}^{-1}$. The average V velocity of the present sample is characteristic of the lag-velocity of thick-disc white dwarfs (Pauli et al. 2006), but it is larger than estimated by Chiba & Beers (2000) for thick-disc stars. On the other hand, the velocity dispersions are intermediate to those of thin- and thick-disc white dwarfs (Pauli et al. 2006). The present NLTT sample is possibly a mix of old thin- and thick-disc populations. Three objects clearly belong to the halo: NLTT 11748, NLTT 31473, and NLTT 33503. NLTT 33503 is a newly identified, young halo white dwarf ($\tau_{\text{cool}} = 170 \text{ Myr}$). We calculated a mass of $0.51 \pm 0.02 M_{\odot}$ and, following the low-metallicity ($Z = 0.0004$) evolutionary models of Girardi et al. (2000), the likely progenitor is a low-mass star ($M \approx 0.85 M_{\odot}$) with a total lifespan of 11 Gyr. NLTT 31473 is an older halo white dwarf ($\tau_{\text{cool}} = 2.9 \text{ Myr}$) with a more massive progen-

itor with a lifespan of 8 Gyr ($M_i \approx 0.94 M_{\odot}$). Two other objects show extreme kinematical properties: the high-field magnetic white dwarf NLTT 13015 and the visual double-degenerate NLTT 17486. Both objects are beyond the 2σ locus of the thick-disc but they are clearly not associated to the halo.

3.5 Comments on selected objects

3.5.1 Overlap with other catalogues or surveys

Our selection is based primarily on the catalogue of Salim & Gould (2003) but some of the targets may also be found in the Liverpool-Edinburgh high proper-motion survey (Pokorny, Jones, & Hambly 2003). Most objects may be found in Luyten’s White Dwarf Catalogues (Luyten 1970, 1977); these objects were considered probable white dwarfs based on their reduced proper-motion but, in most cases, they were awaiting spectroscopic confirmation. Only ten objects were not listed in Luyten’s White Dwarf Catalogues.

A few objects from our sample have been studied previously. Koester et al. (2009) obtained VLT/UVES spectra of NLTT 3080 and measured $(T_{\text{eff}}, \log g) = (6515 \pm 7 \text{ K}, 7.04 \pm 0.01)$. However, by combining $V = 15.26$ from Eggen & Greenstein (1965a) and the 2MASS J , i.e., $V - J = 0.75 \pm 0.04$, we obtain a temperature of $7000 \pm 150 \text{ K}$ in agreement with our spectroscopic determinations (Table 2).

Lamontagne et al. (2000) listed NLTT 5814 as a DA3.5 white dwarf (MCT 0142–3026).

Limoges & Bergeron (2010) measured $(T_{\text{eff}}, \log g) = (10690 \pm 165 \text{ K}, 8.09 \pm 0.06)$ for NLTT 6559 (KUV01552–0703). We obtained a significantly lower surface gravity measurement.

Subasavage et al. (2008) listed NLTT 13532 as a DC white dwarf. However, assuming a hydrogen-rich composition they estimated $T_{\text{eff}} = 5330 \pm 146$ based on optical VRI and 2MASS photometric measurements. We classified NLTT 13532 as a DA white dwarf based on the detection of $H\alpha$ in FORS spectra.

Reid & Gizis (2005) classified the object NLTT 14558 as a DC white dwarf, although a weak $H\alpha$ line is apparent in their spectrum. Based on a photometric temperature estimate, Kawka, Vennes, & Thorstensen (2004) estimated a relatively high tangential velocity. We classified NLTT 14558 as a DA white dwarf based on the detection of $H\beta$ in FORS spectra. The Galactic velocity vectors of NLTT 14558 are typical of the present sample.

Hintzen & Strittmatter (1974) classified NLTT 15957 as a DA “weak” owing to the weak Balmer lines.

Reid & Gizis (2005) classified NLTT 17486 as a DA7 white dwarf. Based on photometric measurements, Subasavage et al. (2008) estimated an effective temperature of $T_{\text{eff}} = 9900 \pm 440 \text{ K}$. Also, Kawka, Vennes, & Thorstensen (2004) estimated a high tangential velocity, and, as noted above (Section 3.4), this object has peculiar kinematics.

NLTT 28493 was classified as a cool DA white dwarf by Kilic et al. (2006). They estimated an effective temperature of $T_{\text{eff}} = 6516 \text{ K}$ using SDSS photometry. Carollo et al. (2006) also showed this star to be a cool DA white dwarf.

For NLTT 33503, Koester et al. (2009) measured $(T_{\text{eff}}, \log g) = (16152 \pm 25 \text{ K}, 7.720 \pm 0.005)$.

Subasavage et al. (2007) classified NLTT 33669 as a DA

white dwarf and estimated $T_{\text{eff}} = 6083 \pm 201$ based on photometry.

Greenstein (1984) classified NLTT 51252 as a DA white dwarf.

NLTT 56805 was classified as a cool DA white dwarf by Vennes & Kawka (2003). They estimated an effective temperature of 4700 ± 300 K, and showed that it has a low surface gravity ($\log g \approx 7$). Our new spectrum along with the SDSS *ugriz* photometry confirm the low temperature. The recent trigonometric parallax measurement of $\pi = 44.9 \pm 2.0$ mas (or $d = 22.3 \pm 1.0$ pc) from Lépine et al. (2009) confirms the low surface gravity of the object: assuming $T_{\text{eff}} = 5000$ K and an absolute magnitude of $M_V = 14.3 \pm 0.1$, we obtain a low surface gravity of $\log g = 7.4 \pm 0.1$.

PM J11480–4523 was selected from the sample of high proper-motion stars of Lépine (2005).

3.5.2 DAZ white dwarfs

Six objects are classified as DAZ white dwarfs. Kawka & Vennes (2011, 2012) already discussed the cases of NLTT 6390, 10480, and 11393. Briefly, they measured calcium abundances ranging from $\log \text{Ca}/\text{H} \approx -10.0$ to -10.5 , and, as mentioned above, measured an averaged surface field of ~ 500 kG in NLTT 10480. The spectrum of NLTT 6390 also showed iron and magnesium lines. Our survey uncovered two new DAZ white dwarfs, NLTT 888 and 7547, and new spectra of NLTT 25792 helped reclassify this object as a DAZ white dwarf. Kilkeny et al. (1997) had originally classified NLTT 25792 (EC 10542–2236) as a sdB+, that is a hot sdB star which shows the Ca K line. Kawka et al. (2011) and Gianninas, Bergeron, & Ruiz (2011) independently identified the star as a cool DAZ white dwarf. Gianninas, Bergeron, & Ruiz (2011) also measured a calcium abundance $\log \text{Ca}/\text{H} = -8.3$ at $T_{\text{eff}} = 7910$ K. Their abundance is somewhat lower than estimated in the present work, and both measurements are lower than estimated by Kawka et al. (2011) because of their higher temperature estimate. Our new measurement of the calcium abundance and effective temperature, $\log \text{Ca}/\text{H} = -7.9 \pm 0.2$ and $T_{\text{eff}} = 7921$, as well as the measurements of Gianninas, Bergeron, & Ruiz (2011) place NLTT 25792 above the observed calcium abundance trend (see Kawka et al. 2011).

The calcium abundances in the atmospheres of NLTT 888 and 7547 are $\log \text{Ca}/\text{H} = -10.65 \pm 0.15$ and -10.05 ± 0.15 , respectively.

3.5.3 Double degenerates and common proper-motion binaries

Several objects are paired with main-sequence or degenerate companions.

The white dwarf NLTT 4615 is in a common proper-motion binary with the dM star NLTT 4616 (Silvestri et al. 2001). They estimated for the white dwarf $T_{\text{eff}} = 6037$ K based on the $V - I$ index. Schilbach & Röser (2012) list NLTT 4615 as a “former” Hyades DC white dwarf. Garcés, Catalán, & Ribas (2011) correctly identified it as a DA white dwarf and measured $T_{\text{eff}} = 5950$ K based on $VJHK$ colours, or ~ 170 K hotter than our spectroscopic measurement.

Silvestri et al. (2001) listed NLTT 7051 as a DA white dwarf and estimated $T_{\text{eff}} = 5709$ K. The white dwarf is in a common proper-motion binary with the dM3 star NLTT 7055.

Gianninas, Bergeron, & Ruiz (2011) independently identified NLTT 21913 as an unresolved DA+DC pair. They found that the binary is composed of a massive DA component with $(T_{\text{eff}}, \log g) = (10000 \text{ K}, 8.91)$ and a cool DC white dwarf with $(T_{\text{eff}}, \log g) = (5600 \text{ K}, 8.00)$. The average of two radial velocity measurements obtained with FORS ($v_r = 95.9 \pm 6.0 \text{ km s}^{-1}$) differs significantly from the velocity measured by Zuckerman et al. (2003) with the Keck HIRES, $v_r = 130.2 \text{ km s}^{-1}$, from which we conclude that NLTT 21913 is a close DA+DC binary. Additional velocity measurements should help constrain the period and DC mass function. We fitted the observed Balmer lines with two sets of model spectra using χ^2 minimization techniques. In each fitting procedure, we varied T_{eff} and $\log g$ for the H-rich white dwarf and only the T_{eff} for the He-rich white dwarf at a given mass. We calculated a set of He-rich spectra at different masses (0.5, 0.6, 0.7 and 0.8 M_{\odot}) and the fitting procedure was repeated for each given mass. We took note of the best χ^2 for each fit and calculated the best mass and temperature for the DC with the corresponding T_{eff} and $\log g$ for the DA white dwarf. Figure 8 (left panel) shows the best fitting model spectra (DA: $T_{\text{eff}} = 9550$, $\log g = 8.58$, $M = 0.96 M_{\odot}$, DC: $T_{\text{eff}} = 6150$, $\log g = 8.11$, $M = 0.63 M_{\odot}$) compared to the observed Balmer lines of NLTT 21913. Similarly, we fitted the spectral energy distribution of NLTT 21913 using the two sets of model spectra. First, we calculated synthetic magnitudes (*GALEX FUV*, *NUV*, *UBV*, and *2MASS JHK*) using our spectra. We then fitted the measured magnitudes *GALEX NUV*, *UBV* and *2MASS J* magnitudes with the synthetic magnitudes assuming a mass of 0.63 M_{\odot} for the DC white dwarf and varying both effective temperatures and the surface gravity of the DA white dwarf. Figure 8 (right panel) shows the measured magnitudes of NLTT 21913 compared to the best fitting combined spectrum and the DA and DC component spectra. Both methods uncovered a massive DA component.

Eggen & Greenstein (1965b) classified NLTT 17662 (EGGR 171) as a DA white dwarf. As discussed earlier (Section 2) we uncovered in the FORS acquisition image a close companion to this object. Both stars were acquired during spectroscopic observations with the bright component (A) centred on the slit and the fainter component (B) off-centre. We measured T_{eff} and $\log g$ of component A using the EFOSC spectrum obtained as part of the P82 programme; component B was left out of the slit. Next, we calculated the absolute R magnitude (M_R) of component A, and, using apparent magnitudes (Table A1) we calculated $M_R = 14.3 \pm 0.3$ mag for component B. Finally, we fitted the H α line profile in the T_{eff} and $\log g$ plane and constrained the range of solutions using the calculated M_R . The resulting parameters are listed in Table 2. The surface gravity or mass measurements are strongly correlated because of the requirement of a constant flux ratio. Component A is hotter and younger than component B. Using the evolutionary models of Schaller et al. (1992) at $Z = 0.019$ and keeping the total age within 10 Gyr, the cooling age differential ($\Delta\tau_{\text{age}} \approx 1.4 - 2.3$ Gyr) implies an initial mass range

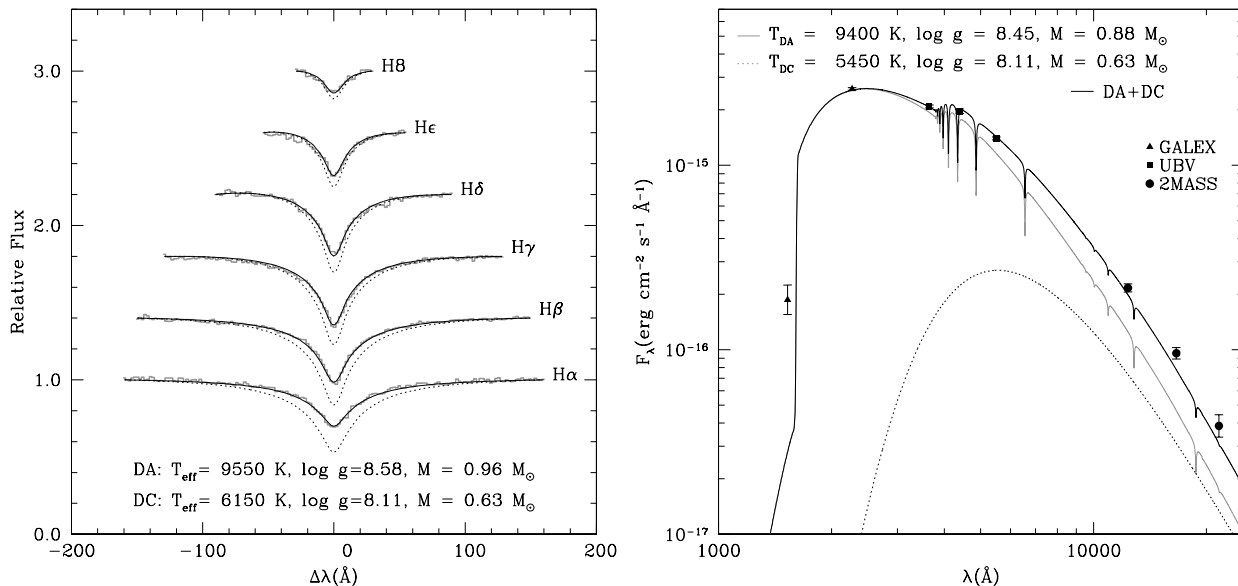


Figure 8. *Left:* Balmer line profiles of NLTT 21913 obtained at CTIO (grey lines) compared to the best fitting model spectrum (full lines) composed of a hydrogen-rich component at $T_{\text{eff}} = 9550$ K, $\log g = 8.58$ (dotted lines) that is diluted by the helium-rich component at $T_{\text{eff}} = 6150$ K, $\log g = 8.11$. *Right:* Photometry of NLTT 21913 (GALEX FUV , $NUV = 20.995 \pm 0.200$, 17.278 ± 0.018 ; $U, B, V = 15.78 \pm 0.02$, 16.32 ± 0.03 , 16.04 ± 0.02 (Kilkenny et al. 1997); 2MASS $J, H, K = 15.401 \pm 0.055$, 15.183 ± 0.077 , 15.111 ± 0.152) compared to the best-fitting spectral energy distribution (full line) showing the contributing fluxes from the hydrogen- and helium-rich components (grey and dotted lines, respectively).

$M_i(A) \approx 1.1 - 2.0 M_{\odot}$ for component A while the cooling age of component B limits the initial mass to $M_i(B) \gtrsim 1.6 M_{\odot}$. Incidentally, the surface gravity measurements suggest that the white dwarf NLTT 17662B is only $0.05 - 0.14 M_{\odot}$ more massive than its companion NLTT 17662A, in agreement with the small gravitational redshift offset between the two stars ($\gamma_B - \gamma_A \approx 6 \text{ km s}^{-1}$). Applying additional constraints stemming from the initial-to-final mass relations of Kalirai et al. (2008), the final mass differential implies an initial mass differential of $\approx 0.4 - 1.3 M_{\odot}$. Hence, the initial, correlated mass ranges are $M_i(A) \approx 1.2 - 1.8 M_{\odot}$ and $M_i(B) \approx 1.6 - 3.1 M_{\odot}$. Further spectroscopic observations, such as a complete Balmer line spectrum of component B, should help refine these estimates.

The white dwarf NLTT 29967 is in a common proper-motion binary with the K-type dwarf HIP 59519 (Gould & Chanemé 2004). The Hipparcos parallax, $\pi = 22.18 \pm 1.49$ mas, corresponds to a distance of $d = 45.1^{+3.2}_{-2.8}$ pc (van Leeuwen 2007) in agreement with our distance estimate of $d = 41 \pm 8$ pc that was obtained using the calculated distance modulus $m - M$. Conversely, by constraining the distance to $45.1^{+3.2}_{-2.8}$ pc and applying the mass-radius relation we constrain the surface gravity to $\log g = 7.92^{+0.14}_{-0.17}$ and the mass to $M = 0.54 \pm 0.09 M_{\odot}$. Garcés, Catalán, & Ribas (2011) measured $(T_{\text{eff}}, \log g) = (6180 \pm 220 \text{ K}, 7.26 \pm 0.45)$ using Balmer line profiles, but $T_{\text{eff}} = 5620 \pm 160$ using photometric measurements alone. Our spectroscopic results confirm the higher temperature estimate.

3.5.4 Halo white dwarfs

Our kinematical study offered clues to the origin (total age) of some of the objects.

Oppenheimer et al. (2001) listed NLTT 5543 as a candidate halo white dwarf and their spectroscopy revealed the presence of the $H\alpha$ line (DA class). Bergeron et al. (2005) estimated an effective temperature of $T_{\text{eff}} = 7000 \pm 180$ K using optical and infrared photometry. We measured $T_{\text{eff}} = 6620 \pm 160$ by fitting the Balmer lines with the surface gravity set to 8.00 ± 0.24 . The effective temperature corresponding to the colour index $V - J = 0.85 \pm 0.11$ is $T_{\text{eff}} = 6640^{+390}_{-340}$ K. The DA NLTT 9940 is the second halo white dwarf candidate proposed by Oppenheimer et al. (2001) that is covered in our sample. Bergeron et al. (2005) estimated $T_{\text{eff}} = 5750 \pm 190$ K based on photometry alone. We measured $T_{\text{eff}} = 5660 \pm 270$ by fitting the Balmer lines, and again setting the surface gravity at 8.00 ± 0.24 . The temperature obtained by fitting the SDSS $ugriz$ colours is 5510 ± 30 K in agreement with the spectroscopic temperature. Both optical-infrared indices ($V - J$ and $R - J$) indicate a lower temperature of 5000 K possibly revealing an error in the 2MASS J band measurement: Kilic et al. (2010) measured $J = 16.20$ and the optical-infrared index $V - J = 1.13$ corresponds to a temperature of ≈ 5800 K in agreement with optical temperatures. We confirm that neither object, NLTT 5543 or NLTT 9940, is a genuine halo white dwarf but, instead, they are likely members of the thick-disc (see also Salim et al. 2004).

We originally presented evidence of the peculiar Galactic velocity components of NLTT 11748 (Kawka & Vennes 2009; Kawka, Vennes, & Vaccaro 2010). Its halo member-

ship also allowed Kawka & Vennes (2009) to constrain the mass of the progenitor ($M_i \approx 0.9 M_\odot$). The DA white dwarfs NLTT 31473 and NLTT 33503 are two new candidates for the halo membership based on their Galactic velocity components (Fig. 7).

4 SUMMARY AND DISCUSSION

We have conducted a spectropolarimetric survey of 58 DA white dwarfs. We report the discovery of the low-field magnetic white dwarf NLTT 2219 ($B_l = -97$ kG) and of the likely extremely low-field white dwarf NLTT 347. Our survey also led to the identification of the magnetic DAZ white dwarf NLTT 10480 (Kawka & Vennes 2011). Spectropolarimetric series of the high-field white dwarf NLTT 12758 revealed short-period ($\lesssim 1$ hr) polarity variations characteristic of a rotating dipole. We also noted radial velocity variations and a strong contrast in the strengths of the π and σ components suggesting that NLTT 12758 is a spectroscopic binary. Further work on this object is awaiting detailed Zeeman modelling and additional spectroscopic data to establish the periodicity of the radial velocity and field variations. The time series of NLTT 13015 also showed possible variations and the surface-averaged field spread from 6 to 7.5 MG. The precision of $H\alpha$ velocity measurements also allowed us to identify potential close double degenerate stars such as the DA+DC NLTT 21913 and the single-lined DA white dwarfs NLTT 6559 and NLTT 31473. Incidentally, NLTT 31473 is also a member of the Galactic halo. Maxted & Marsh (1999) used their radial velocity survey to determine the fraction of double degenerate systems among white dwarfs to be between $\sim 2\%$ and 19% . Including the likely double-degenerate NLTT 12758, we estimate the fraction of close double degenerates at $7 \pm 3\%$.

We exploited the present data to infer stellar (mass, age) and kinematical properties of this sample of relatively old high-proper motion white dwarfs. For instance, we identified two new halo white dwarf candidates (NLTT 31473 and NLTT 33503) among a sample of thin- or thick-disc white dwarfs.

The atmospheric parameters (T_{eff} and $\log g$) obtained using spectroscopic and photometric data are in good agreement. The SDSS *ugriz* photometry allowed us for the first time to assess the effect of $\text{Ly}\alpha$ extended-wing opacities (Kowalski & Saumon 2006) on the SDSS $u - g$ colour index of cool DA white dwarfs.

The incidence of magnetism in white dwarfs has been reported to be as low as 4% (Schmidt & Smith 1995) when taking into account all magnetic field strengths, or $\sim 1\%$ per decade interval. However, it was reported to be as high as 25% when considering only the very low-field white dwarfs (Aznar Cuadrado et al. 2004). Aznar Cuadrado et al. (2004) detected kG fields in three white dwarfs out of total 12, and when they extended their survey to an additional 10 objects they only reported one possible candidate (Jordan et al. 2007). The combined survey hence reduced the incidence of kG fields in white dwarfs to 11 - 15%. Kawka et al. (2007) studied the incidence of magnetism in the Solar neighbourhood and found that $21\% \pm 8\%$ of white dwarfs are magnetic. In the present survey of nearly 60 objects we uncovered three new low-field

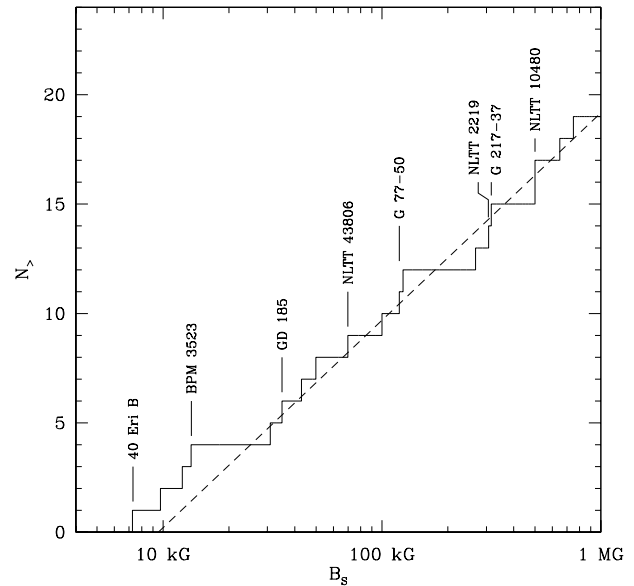


Figure 9. Cumulative distribution of low-field measurements ($B_s \lesssim 1\text{MG}$) in white dwarfs, where $N_>$ is the number of objects with a field larger than a surface average field B_s . Notable objects from Table 5 are marked. With the exception of a slight enhancement near 10 kG, the observed distribution is nearly linear implying a constant incidence of magnetic field per decade.

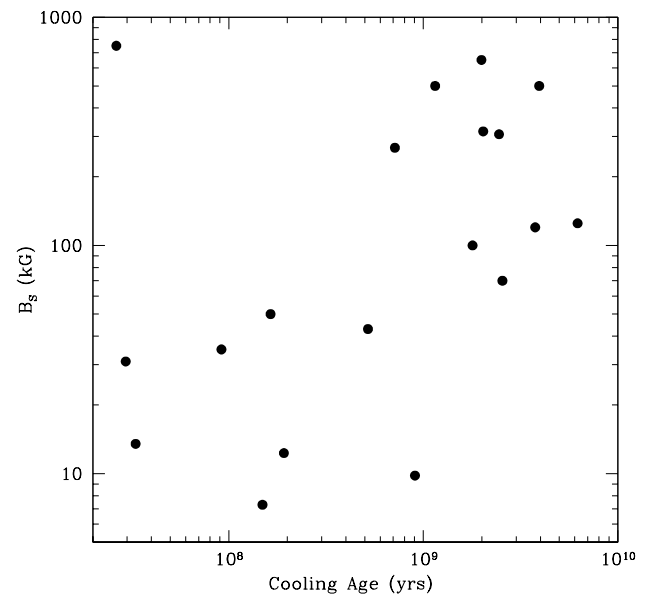


Figure 10. Magnetic field strength versus cooling age for low-field white dwarfs (Table 5).

white dwarfs with strengths of the order of ~ 10 to $\sim 10^2$ kG implying a field incidence of $5 \pm 2\%$, or $\sim 1 - 2\%$ per decade interval. The incidence observed in the present sample is similar to that observed by Schmidt & Smith (1995).

The exact fraction remains uncertain because of inhomogeneous sampling and methodology. Figure 9 shows the

cumulative distribution of low-field white dwarfs as a function of the field logarithm. The linear relation corresponds to a nearly flat distribution and is evidence that fields are distributed randomly rather than following a distribution pattern as found in Ap stars (Aurière et al. 2007). Fields generated by a dynamo involving a common-envelope phase (see Tout et al. 2008; Potter & Tout 2010; Nordhaus et al. 2011) with a body varying in size, hence disposable energy, such as an asteroid, a planet, a brown dwarf, or a low-mass star are likely to vary in intensity as well. The random nature of the size of the body involved in the common-envelope phase should also result in random field intensity. Once the field is frozen into the stellar body, the decay time-scale is of the order of $10^9 - 10^{10}$ years (Muslimov et al. 1995), i.e., comparable to the white dwarf cooling age. On the other hand, the Ap stars are still likely progenitors of high-field ($\gtrsim 10^7$ G) white dwarfs.

Are two independent formation channels possible? Tout et al. (2008) argues that the absence of magnetic white dwarfs in non-interacting pairs implies that all magnetic white dwarfs are the products of interaction or merger. This syllogism does not exclude other possible channels if it can be shown that the failure to identify magnetic white dwarfs in non-interacting binaries is the result of a selection effect for this particular channel. For example, Carrier et al. (2002) found that $\sim 40\%$ of Ap stars are in binaries. The inferred distribution of mass ratios implies that close to half of the progeny of Ap stars, i.e., the high-field magnetic white dwarfs, would be paired with luminous companions (G- to A-type) hence escaping detection, although the remainder would be paired with M- to K-type stars and should be detectable, at least during the early cooling stages. As noted by Tout et al. (2008), late-type companions remain elusive, but it remains to be shown that early-type companions are missing as well.

The stellar ages in this sample vary from 20 Myr to 5 Gyr. The distribution of field strengths as a function of temperatures possibly reveals strong selection effects in the sample. Figure 10 shows that all stars from Table 5 and with a field ≤ 50 kG are relatively young stars with cooling ages $\lesssim 10^9$ years. Conversely, all stars save two with a field stronger than 50 kG are older stars with cooling ages in excess of $\sim 10^9$ years. Deep, narrow spectral lines are reliable field tracers but are also lacking in cool white dwarfs unless heavy element lines are present such as in the magnetic DAZ NLTT 43806 (Zuckerman et al. 2011) or NLTT 10480 (Kawka & Vennes 2011). On the other hand, an explanation for the paucity of intermediate fields (100 kG–1 MG) in younger white dwarfs is not readily available. Although these are the field and temperature ranges targeted in most spectropolarimetric surveys (see, e.g., Aznar Cuadrado et al. 2004), a larger survey may yet uncover the missing objects.

ACKNOWLEDGMENTS

S.V. and A.K. acknowledge support from the Grant Agency of the Czech Republic (GA ČR P209/10/0967 and GA ČR P209/12/0217). A.K. also acknowledges support from the Centre for Theoretical Astrophysics (LC06014). This work was also supported by the project RVO:67985815.

Table 5. Low-field ($B_S \lesssim 1$ MG) white dwarfs.

Name	T_{eff} (K)	Age ^a (Gyr)	B_S (kG)	Method ^b	Ref. ^c
40 Eri B	16500	0.15	7.3	B_1	1
LTT 9857	8660	0.91	9.8	B_1	2
LTT 4099	15280	0.19	12.3	B_1	2
BPM 3523	23450	0.03	13.5	B_1	2
2329–291	24000	0.03	31.	B_S	3
1531–022	18850	0.09	35.	B_S	3
2105–820	10760	0.52	43.	B_S	3
2039–682	16050	0.16	50.	B_S	3
NLTT 43806	5900	2.55	70.	B_S	4
LHS 5064	6680	1.79	100.	B_S	5
G 77-50	5310	3.76	120.	B_S	6
G 234-4	~ 4500	6.21	125.	B_1	7
LP 907-37	~ 9500	0.71	268.	B_1	8
NLTT 2219	5980	2.45	307.	B_1	9
G 217-37	~ 6400	2.03	316.	B_1	8
1953–011	~ 7900	1.15	500. ^d	B_S	10
NLTT 10480	~ 5250	3.94	500.	B_S	11
G 165-7	6440	1.99	650.	B_S	12
LB 8915	~ 24500	0.03	750.	B_S	13

^a Calculated assuming $\log g = 8$.

^b Original measurement from spectropolarimetry (B_1) or spectroscopy (B_S). The equivalent B_S is estimated at $i = 57^\circ$, i.e., $B_S \approx 3.16 \times B_1$.

^c References: 1 - Fabrika et al. (2000); 2 - Aznar Cuadrado et al. (2004); 3 - Koester et al. (1998); 4 - Zuckerman et al. (2011); 5 - Bergeron, Ruiz, & Leggett (1997); 6 - Farihi et al. (2011); 7 - Putney (1997); 8 - Schmidt & Smith (1994); 9 - this work; 10 - Maxted et al. (2000); 11 - Kawka & Vennes (2011); 12 - Dufour et al. (2006); 13 - Wesemael et al. (2001).

^d Highest of the two components.

This publication makes use of data products from the Two Micron All Sky Survey, which is a joint project of the University of Massachusetts and the Infrared Processing and Analysis Center/California Institute of Technology, funded by the National Aeronautics and Space Administration and the National Science Foundation. This publication also makes use of SDSS spectroscopic and photometric data. Funding for SDSS-III has been provided by the Alfred P. Sloan Foundation, the Participating Institutions, the National Science Foundation, and the U.S. Department of Energy Office of Science. SDSS-III is managed by the Astrophysical Research Consortium for the Participating Institutions of the SDSS-III Collaboration.

REFERENCES

- Aurière M. et al., 2007, *A&A*, 475, 1053
 Aznar Cuadrado R., Jordan S., Napiwotzki R., Schmid H. M., Solanki S. K., Mathys G., 2004, *A&A*, 423, 1081
 Bagnulo, S., Szeifert T., Wade G.A., Landstreet J.D., Mathys, G., 2002, *A&A*, 389, 191
 Barstow M. A., Jordan S., O’Donoghue D., Burleigh M. R., Napiwotzki R., Harrop-Allin M. K., 1995, *MNRAS*, 277, 971
 Benvenuto, O.G., Althaus, L.G., 1999, *MNRAS*, 303, 30

- Bergeron P., Ruiz M.T., Hamuy M., Leggett S.K., Currie M.J., Lajoie C.-P., Dufour, P., 2005, *ApJ*, 625, 838
- Bergeron P., Ruiz M. T., Leggett S. K., 1997, *ApJS*, 108, 339
- Brinkworth C. S., Marsh T. R., Morales-Rueda L., Maxted P. F. L., Burleigh M. R., Good S. A., 2005, *MNRAS*, 357, 333
- Burleigh M. R., Jordan S., Schweizer W., 1999, *ApJ*, 510, L37
- Carollo D., Bucciarelli B., Hodgkin S.T., et al., 2006, *A&A*, 448, 579
- Carrier F., North P., Udry S., Babel J., 2002, *A&A*, 394, 151
- Chiba M., Beers T. C., 2000, *AJ*, 119, 2843
- Costa E., Méndez R. A., Jao W.-C., Henry T. J., Subasavage J. P., Ianna P. A., 2006, *AJ*, 132, 1234
- Dobbie P. D., Baxter R., Külebi B., Parker Q. A., Koester D., Jordan S., Lodieu N., Euchner F., 2012, *MNRAS*, 421, 202
- Dufour P., Bergeron P., Schmidt G. D., Liebert J., Harris H. C., Knapp G. R., Anderson S. F., Schneider D. P., 2006, *ApJ*, 651, 1112
- Eggen O.J., 1968, *ApJ*, 153, 195
- Eggen O. J., Greenstein J. L., 1965a, *ApJ*, 141, 83
- Eggen O. J., Greenstein J. L., 1965b, *ApJ*, 142, 925
- Fabrika S. N., Valyavin G. G., Burlakova T. E., Barsukova E. A., Monin D. N., 2000, in *Magnetic Fields of Chemically Peculiar and Related Stars*, ed. Yu. V. Glogolevskij & I. I. Romanyuk, (Moscow: Russian Acad. Sci.) 218
- Farihi J., Dufour P., Napiwotzki R., Koester D., 2011, *MNRAS*, 413, 2559
- Ferrario L., Vennes S., Wickramasinghe D. T., Bailey J. A., Christian D. J., 1997, *MNRAS*, 292, 205
- Garcés A., Catalán S., Ribas I., 2011, *A&A*, 531, A7
- García-Berro E., et al., 2012, *ApJ*, 749, 25
- Garstang R. H., Kemic S. B., 1974, *Ap&SS*, 31, 103
- Giammichele N., Bergeron P., Dufour, P., 2012, *ApJS*, 199, 29
- Gianninas A., Bergeron P., Ruiz M. T., 2011, *ApJ*, 743, 138
- Girardi L., Bressan A., Bertelli G., Chiosi C., 2000, *A&AS*, 141, 371
- Girven J., Gänsicke B. T., Külebi B., Steeghs D., Jordan S., Marsh T. R., Koester D., 2010, *MNRAS*, 404, 159
- Gould, A. Chanamé, J., 2004, *ApJS*, 150, 455
- Greenstein J. L., 1984, *ApJ*, 276, 602
- Hintzen P., Strittmatter P. A., 1974, *ApJ*, 193, L111
- Johnson D. R. H., Soderblom D. R., 1987, *AJ*, 93, 864
- Jordan S., 1992, *A&A*, 265, 570
- Jordan S., Aznar Cuadrado R., Napiwotzki R., Schmid H. M., Solanki S. K., 2007, *A&A*, 462, 1097
- Kalirai J. S., Hansen B. M. S., Kelson D. D., Reitzel D. B., Rich R. M., Richer H. B., 2008, *ApJ*, 676, 594
- Kawka A., Vennes S., 2004, in *A-Star Puzzle* (Cambridge University Press), ed. J. Zverko, J. Ziznovsky, S. J. Adelman, & W.W. Weiss, *Proc. IAU Symp.*, 224, 879
- Kawka A., Vennes S., 2006, *ApJ*, 643, 402
- Kawka A., Vennes S., 2009, *A&A*, 506, L25
- Kawka A., Vennes S., 2011, *A&A*, 532, A7
- Kawka A., Vennes S., 2012, *A&A*, 538, A13
- Kawka A., Vennes S., Dinnbier F., Cibulková H., Németh P., 2011, *AIP Conf. Ser.*, 1331, 238
- Kawka A., Vennes S., Schmidt G. D., Wickramasinghe D. T., Koch R., 2007, *ApJ*, 654, 499
- Kawka A., Vennes S., Thorstensen J. R., 2004, *AJ*, 127, 1702
- Kawka A., Vennes S., Vaccaro T. R., 2010, *A&A*, 516, L7
- Kemic S. B., 1974, *ApJ*, 193, 213
- Kepler S. O., Kleinman S. J., Nitta A., Koester D., Castanheira B. G., Giovannini O., Costa A. F. M., Althaus L., 2007, *MNRAS*, 375, 1315
- Kilic M., et al., 2010, *ApJS*, 190, 77
- Kilic M., Munn J. A., Harris H. C., et al., 2006, *AJ*, 131, 582
- Kilkenny D., O'Donoghue D., Koen C., Stobie R.S., Chen A., 1997, *MNRAS*, 287, 867
- Kleinman S. J., et al., 2004, *ApJ*, 607, 426
- Koester D., Dreizler S., Weidemann V., Allard N. F., 1998, *A&A*, 338, 612
- Koester D., Voss B., Napiwotzki R., Christlieb N., Homeier D., Lisker T., Reimers D., Heber U., 2009, *A&A*, 505, 441
- Kowalski P. M., Saumon D., 2006, *ApJ*, 651, L137
- Lamontagne R., Demers S., Wesemael F., Fontaine G., Irwin M. J., 2000, *AJ*, 119, 241
- Lépine S., 2005, *AJ*, 130, 1247
- Lépine S., Thorstensen J. R., Shara M. M., Rich R. M., 2009, *AJ*, 137, 4109
- Limoges M.-M., Bergeron P., 2010, *ApJ*, 714, 1037
- Luyten W. J., 1970, *White dwarfs* (Minneapolis: Univ. Minnesota Press)
- Luyten W.J., 1977, *White Dwarfs II* (Minneapolis: Univ. Minnesota Press)
- Martin B., Wickramasinghe D. T., 1984, *MNRAS*, 206, 407
- Maxted P.F.L., Ferrario L., Marsh T. R., Wickramasinghe, D. T., 2000, *MNRAS*, 315, L41
- Maxted P. F. L., Marsh T. R., 1999, *MNRAS*, 307, 122
- McCook G. P. Sion E. M., 1999, *ApJS*, 121, 1
- Muslimov A. G., Van Horn H. M., Wood, M. A., 1995, *ApJ*, 442, 758
- Nordhaus J., Wellons S., Spiegel D. S., Metzger B. D., Blackman E. G., 2011, *Proc. National Academy of Science*, 108, 3135
- Oppenheimer B. R., Hambly N. C., Digby A. P., Hodgkin S. T., Saumon D., 2001, *Science*, 292, 698
- Patat F., et al., 2011, *A&A*, 527, A91
- Pauli E.-M., Napiwotzki R., Heber U., Altmann M., Odenkirchen M., 2006, *A&A*, 447, 173
- Pokorny R. S., Jones H. R. A., Hambly N. C., 2003, *A&A*, 397, 575
- Potter A. T., Tout C. A., 2010, *MNRAS*, 402, 1072
- Putney A., 1997, *ApJS*, 112, 527
- Reid, I.N. & Gizis, J.E. 2005, *PASP*, 117, 676
- Salim S., Gould A., 2003, *ApJ*, 582, 1011
- Salim S., Rich R. M., Hansen B. M., Koopmans L. V. E., Oppenheimer B. R., Blandford R. D., 2004, *ApJ*, 601, 1075
- Schaller G., Schaerer D., Meynet G., Maeder A., 1992, *A&AS*, 96, 269
- Schilbach E., Röser S., 2012, *A&A*, 537, A129
- Schmidt G. D., et al., 2003, *ApJ*, 595, 1101
- Schmidt G. D., Smith P. S., 1994, *ApJ*, 423, L63
- Schmidt G. D., Smith P. S. 1995, *ApJ*, 448, 305
- Serenelli A. M., Althaus L. G., Rohrmann R. D., Benvenuto O. G., 2002, *MNRAS*, 337, 1091

- Silvestri N. M., Oswalt T. D., Wood M. A., Smith J. A., Reid I. N., Sion E. M., 2001, *AJ*, 121, 503
 Skrutskie M. F., et al., 2006, *AJ*, 131, 1163
 Smith, J. A. 1997, Ph.D. Thesis, Florida Institute of Technology
 Subasavage, J.P., Henry, T.J., Bergeron, P., Dufour, P., Hambly, N.C., & Beaulieu, T.D. 2007, *AJ*, 134, 252
 Subasavage, J.P., Henry, T.J., Bergeron, P., Dufour, P., & Hambly, N.C. 2008, *AJ*, 136, 899
 Tout C. A., Wickramasinghe D. T., Liebert J., Ferrario L., Pringle J. E., 2008, *MNRAS*, 387, 897
 Tremblay, P.-E., Bergeron, P., & Gianninas, A. 2011, *ApJ*, 730, 128
 Valyavin G., Wade G. A., Bagnulo S., Szeifert T., Landstreet J. D., Han I., Burenkov A., 2008, *ApJ*, 683, 466
 van Leeuwen F., 2007, *A&A*, 474, 653
 Vennes S., Ferrario L., Wickramasinghe D. T., 1999, *MNRAS*, 302, L49
 Vennes, S. & Kawka, A. 2003, *ApJ*, 586, L95
 Vennes S., Schmidt G. D., Ferrario L., Christian D. J., Wickramasinghe D. T., Kawka A., 2003, *ApJ*, 593, 1040
 Vergely J.-L., Freire Ferrero R., Siebert A., Valette B., 2001, *A&A*, 366, 1016
 Welsh B. Y., Lallement R., Vergely J.-L., Raimond S., 2010, *A&A*, 510, A54
 Wesemael F., Liebert J., Schmidt G. D., Beauchamp A., Bergeron P., Fontaine G., 2001, *ApJ*, 554, 1118
 Wickramasinghe D. T., Ferrario L., 2005, *MNRAS*, 356, 1576
 Zuckerman B., Koester D., Dufour P., Melis C., Klein B., Jura M., 2011, *ApJ*, 739, 101
 Zuckerman B., Koester D., Reid I. N., Hüensch M., 2003, *ApJ*, 596, 477

APPENDIX A: PHOTOMETRIC DATA

Images obtained during our P82 and P83 EFOSC programmes were obtained with either the V filter or the R filter. We employed a subset of stars also listed in the SDSS photometric survey to calibrate the EFOSC images. First, we computed synthetic relations between the SDSS g and r and the Johnson V and R magnitudes. Using a sequence of models at $0.6 M_{\odot}$ and $T_{\text{eff}} = 5$ to 20×10^3 K we obtained

$$V = r + 0.46 \times (g - r) - 0.069,$$

$$R = r - 0.13 \times (g - r) - 0.191,$$

and converted the set of SDSS gr magnitudes from Table A2 into Johnson V and R magnitudes. Next, we measured the count rates c from the acquisition images and calculated the instrumental magnitudes:

$$V(R)_{\text{acq.}} = -2.5 \log c + 25.$$

Finally, simple linear relations were found between $V(R)$ and $V(R)_{\text{acq.}}$ using the SDSS sample:

$$V(R)_{\text{EFOSC}} \equiv V(R) = V(R)_{\text{acq.}} + C_{V(R)},$$

with standard deviations ≈ 0.01 mag for V and 0.03 mag for R . Having estimated the constants C_V and C_R , the calibration was applied to the whole EFOSC sample to measure V and R magnitudes. The uncertainty on the R magnitude of

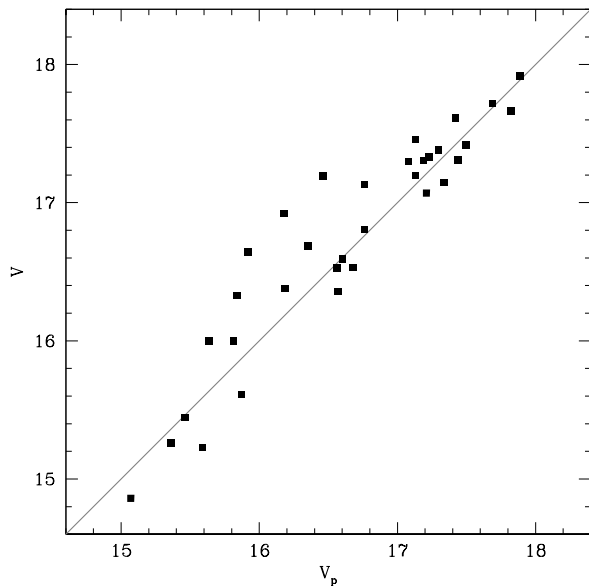


Figure A1. Photographic visual magnitudes (V_p) from the rNLTT catalogue of Salim & Gould (2003) versus calibrated CCD photometry (V) from Table A1.

the faint companion to NLTT 17662 is larger at 0.05 mag. We employed airmass coefficients averaged over the V and R bands, $k_V \approx 0.13$ and $k_R \approx 0.10$ (Patat et al. 2011). The new magnitudes are listed in Table 1 along with published V magnitudes and 2MASS J magnitudes (Skrutskie et al. 2006).

The images obtained during our P80 and P84 FORS programmes were obtained in white light. The CCD employed for the P80 observations was more sensitive in the blue and appropriate to estimate V magnitudes, while the CCD employed for the P84 observations was appropriate to estimate R magnitudes. We followed the procedure outlined above to calibrate the FORS images. The standard deviations were 0.04 and 0.03 mag for the V and R calibration stars, respectively.

Figure A1 shows photographic (V_p Salim & Gould 2003) and CCD photometric measurements (V) from our sample of stars. The photographic measurements are on average 0.1 mag brighter than the CCD measurements with a standard deviation of 0.29 mag.

Figure A2 shows the measured and synthetic $V - J$ and $R - J$ indices as a function of temperature. The blended 2MASS J measurements of the resolved binaries NLTT 17662 and NLTT 56045, and the composite colours of the close binary NLTT 21913 were excluded from the diagrams. The adopted effective temperature measurements are from Table 2. Excluding NLTT 11748¹, the average deviation between predicted and measured $V - J$ is +0.046 mag with a standard deviation of 0.096 mag, while the average deviation for the $R - J$ index is +0.007 with a standard de-

¹ The spectral energy distribution of the extremely low-mass white dwarf NLTT 11748 shows the effect of reddening ($E_{B-V} = 0.1$, Kawka & Vennes 2009)

Table A1. Optical and infrared magnitudes.

Name	EFOSC		FORS		Published		2MASS
	<i>V</i>	<i>R</i>	<i>V</i>	<i>R</i>	<i>V</i> (σ_V)	Ref. ^a	<i>J</i> (σ_J)
NLTT 82	16.53	...		16.120(0.093)
NLTT 347	16.77	...		16.163(0.094)
NLTT 888	17.669	...	17.659		16.478(0.104)
NLTT 2219	17.297	...	17.307		16.392(0.096)
NLTT 2886	16.57	...		15.901(0.091)
NLTT 3080	15.26(0.05)	1	14.506(0.033)
NLTT 3471	16.593	16.43	...		16.445(0.123)
NLTT 4615	17.440	17.09	17.48(0.02)	2	16.461(0.092)
NLTT 5503	16.26	...		16.276(0.087)
NLTT 5543	17.137	...	17.127	...	17.18(0.03)	3	16.296(0.091)
NLTT 5814	16.43	...		16.531(0.101)
NLTT 6004	16.329		15.597(0.060)
NLTT 6390	17.265	...	17.33(0.04)	4	16.355(0.128)
NLTT 6559	16.357	16.24	...		16.272(0.106)
NLTT 6794	16.99	...		16.528(0.113)
NLTT 7051	16.47	16.92(0.02)	2	15.536(0.055)
NLTT 7547	17.946	...	17.910		16.636(0.133)
NLTT 8432	16.91	...		16.190(0.091)
NLTT 9940	17.309	16.97	17.35(0.03)	3	15.819(0.081) ^b
NLTT 10480	17.380	17.49(0.05)	5	16.003(0.078)
NLTT 10884	17.195		16.666(0.138)
NLTT 11393	17.070	17.16(0.04)	4	16.036(0.084)
NLTT 11748	16.656	16.44	...		15.837(0.077)
NLTT 12758	15.446	15.46(0.05)	6	14.809(0.032)
NLTT 12796	16.14	...		16.039(0.078)
NLTT 13015	17.417	17.10	...		16.297(0.111)
NLTT 13471	16.72	...		15.998(0.078)
NLTT 13532	16.33	...		15.369(0.050)
NLTT 13755	16.83(0.25)	7	15.983(0.063)
NLTT 14491	17.194		16.315(0.100)
NLTT 14558	17.717		16.466(0.120)
NLTT 15882	16.85	...		16.107(0.080)
NLTT 15957	16.804		16.064(0.076)
NLTT 17486	...	15.503	...	15.44	15.61(0.03)	8	15.485(0.063)
NLTT 17662A	...	15.795		15.435(0.056)
NLTT 17662B	...	16.82
NLTT 17874	...	16.433	...	16.48	...		15.711(0.073)
NLTT 21844	...	16.349	16.643		15.989(0.066)
NLTT 21913A+B	16.04(0.02)	9	15.401(0.055)
NLTT 23966	16.89	17.13(0.04)	4	16.544(0.112)
NLTT 24406	...	17.121	...	17.02	...		16.421(0.107)
NLTT 25792	15.998		15.521(0.050)
NLTT 28493	16.359	...	16.39(0.03)	10	15.543(0.060)
NLTT 28730	...	16.310	16.529		16.207(0.082)
NLTT 29967	...	16.711		16.018(0.087)
NLTT 31473	16.15	16.53(0.02)	11	15.354(0.047)
NLTT 31483	...	17.148	17.614		16.592(0.113)
NLTT 32785	16.79	...		15.833(0.062)
NLTT 33503	14.86(0.02)	9	15.172(0.049)
NLTT 33669	16.689		15.563(0.051)
NLTT 35570	16.71	...		16.139(0.092)
NLTT 38356	17.309		16.560(0.130)
NLTT 50161	16.99	...		16.789(0.118)
NLTT 51252	15.230	15.23(0.05)	12	15.606(0.060)
NLTT 56045A	16.55	...		16.390(0.113)
NLTT 56045B	17.64

^a References: 1 - Eggen & Greenstein (1965a); 2 - Smith (1997); 3 - Bergeron et al. (2005); 4 - Kawka & Vennes (2012); 5 - Kawka & Vennes (2011); 6 - Eggen (1968); 7 - Salim & Gould (2003); 8 - Subasavage et al. (2008); 9 - Kilkenny et al. (1997); 10 - Subasavage et al. (2007); 11 - Costa et al. (2006); 12 - Greenstein (1984); 13 - Lépine et al. (2009); 14 - Lépine (2005).

^b Kilic et al. (2010) measured $J = 16.20 \pm 0.04$.

Table A1 – continued

Name	EFOSC		FORS		Published		2MASS
	V	R	V	R	V (σ_V)	Ref. ^a	J (σ_J)
NLTT 56257	15.46	...		15.217(0.035)
NLTT 56493	17.05	...		15.772(0.063)
NLTT 56805	15.976	...	15.977	...	16.05(0.05)	13	14.512(0.034)
PMJ11480–4523	15.66(0.25)	14	14.888(0.039)

^a References: 1 - Eggen & Greenstein (1965a); 2 - Smith (1997); 3 - Bergeron et al. (2005); 4 - Kawka & Vennes (2012); 5 - Kawka & Vennes (2011); 6 - Eggen (1968); 7 - Salim & Gould (2003); 8 - Subasavage et al. (2008); 9 - Kilikenny et al. (1997); 10 - Subasavage et al. (2007); 11 - Costa et al. (2006); 12 - Greenstein (1984); 13 - Lépine et al. (2009); 14 - Lépine (2005).

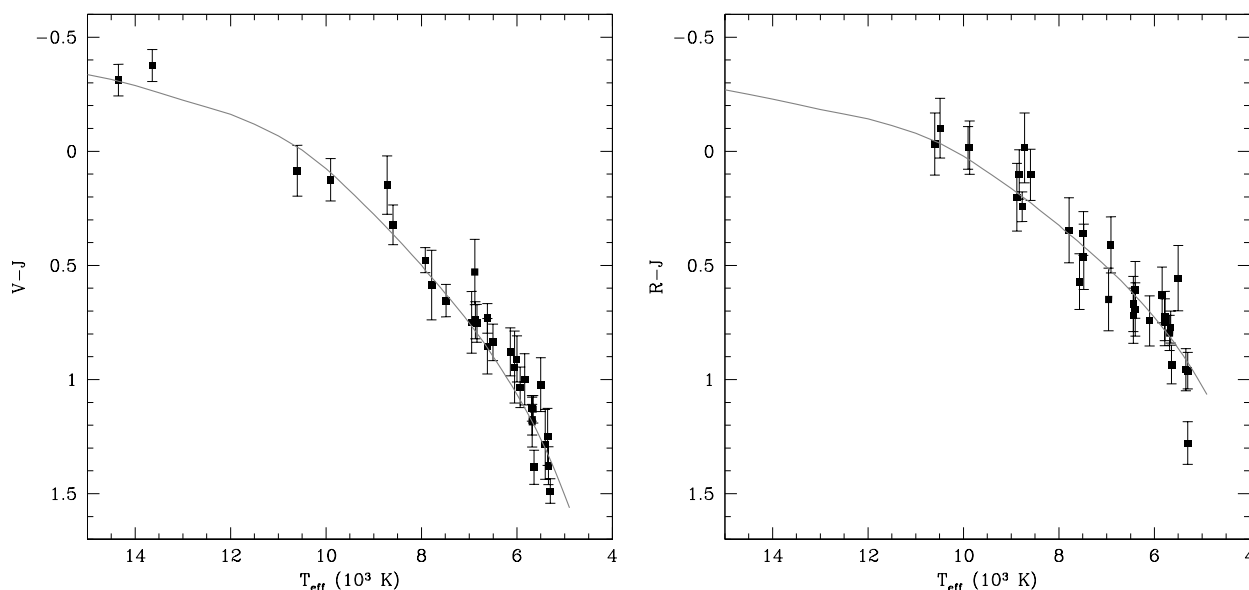


Figure A2. Photometric $V - J$ (left panel) and $R - J$ (right panel) indices as a function of effective temperatures measured using Balmer line profiles. The synthetic relations (grey lines) may be employed to obtain photometric temperature estimates.

viation of 0.119 mag. Applying the synthetic relations to the data, again excluding NLTT 11748, we calculated a reduced χ^2 of ~ 1.2 in the $R - J$ diagram and ~ 1.3 in the $V - J$ diagram. The effect of crowded companions or dust is likely to affect the colours of a few of the outliers found in these diagrams. We noted a discrepancy of ~ 0.4 mag between the 2MASS J magnitude of NLTT 9940 and the $J = 16.20 \pm 0.04$ measurement of Kilic et al. (2010). Opting for the latter, the revised $V - J$ and $R - J$ indices are in excellent agreement with the optical temperatures (see Section 3.5.4). We conclude that errors in optical and infrared magnitudes account for the dispersion. However, the $R - J$ index of NLTT 56493 reveals an object markedly redder than expected suggesting a possible contamination of the 2MASS J measurement.

APPENDIX B: RADIAL VELOCITY MEASUREMENTS

Table B1 list individual heliocentric velocity measurements using the $H\alpha$ line. Quoted errors are statistical only, i.e., follow from the line core fit. We recommend to add 5 km s^{-1} in quadrature to account for accidental shifts in the wavelength scale from night-to-night. The velocities are measured relative to $H\alpha$ ($\lambda_0 = 6562.80\text{\AA}$) in non-magnetic stars and relative to the shifted π component of $H\alpha$ computed at the appropriate field strength in NLTT 13015 ($\lambda_\pi = 6560.43\text{\AA}$). The velocity measurements of NLTT 17662B were corrected by adjusting the telluric lines of the B component with that of the A component because the spectra were obtained with the A component centred on the slit and the B component significantly off-centre. We calculated and applied a correction of $+34.4 \text{ km s}^{-1}$ to the spectra of NLTT 17662B.

Table A2 lists SDSS photometric data depicted in Figure 3.

Table A2. SDSS photometry.

NLTT	SDSS	<i>u</i>	<i>g</i>	<i>r</i>	<i>i</i>	<i>z</i>
82	J000410.41-034008.5	17.449 ± 0.010	16.917 ± 0.005	16.742 ± 0.005	16.708 ± 0.006	16.728 ± 0.009
888	J001737.86-051649.6	19.011 ± 0.028	17.983 ± 0.006	17.536 ± 0.006	17.352 ± 0.006	17.344 ± 0.017
2219	J004056.24-080912.4	18.442 ± 0.020	17.575 ± 0.005	17.208 ± 0.005	17.106 ± 0.006	17.069 ± 0.012
3471	J010319.70-032501.0	17.036 ± 0.008	16.646 ± 0.004	16.659 ± 0.005	16.705 ± 0.005	16.812 ± 0.010
4615	J012314.84-020926.9	18.690 ± 0.022	17.729 ± 0.005	17.306 ± 0.005	17.158 ± 0.006	17.148 ± 0.015
5503	J013852.65-035650.9	16.793 ± 0.008	16.351 ± 0.004	16.441 ± 0.004	16.552 ± 0.005	16.730 ± 0.009
6559	J015742.08-064847.8	16.830 ± 0.009	16.363 ± 0.004	16.476 ± 0.005	16.579 ± 0.005	16.839 ± 0.011
7547	J021719.98-065628.5	19.677 ± 0.037	18.323 ± 0.007	17.746 ± 0.006	17.528 ± 0.007	17.440 ± 0.014
9940	J030713.90-071506.1	18.698 ± 0.020	17.635 ± 0.005	17.179 ± 0.005	16.988 ± 0.006	16.937 ± 0.014
17874	J072704.21+143439.5	18.202 ± 0.014	17.135 ± 0.005	16.692 ± 0.005	16.515 ± 0.006	16.455 ± 0.008
21844	J092840.28+184113.6	17.095 ± 0.008	16.696 ± 0.004	16.580 ± 0.005	16.574 ± 0.005	16.676 ± 0.009
24406	J102747.63+192824.1	17.881 ± 0.013	17.387 ± 0.005	17.228 ± 0.005	17.178 ± 0.005	17.254 ± 0.012
25792	J105638.59-225254.3	16.540 ± 0.007	16.079 ± 0.004	15.974 ± 0.004	15.984 ± 0.005	16.062 ± 0.007
28493	J114625.77-013636.9	17.119 ± 0.008	16.499 ± 0.004	16.235 ± 0.003	16.152 ± 0.004	16.146 ± 0.007
31473	J124024.15-231743.9	17.917 ± 0.013	16.814 ± 0.004	16.337 ± 0.004	16.151 ± 0.004	16.084 ± 0.007
31483	J124030.26+180728.2	19.201 ± 0.023	17.990 ± 0.007	17.416 ± 0.006	17.193 ± 0.006	17.114 ± 0.011
56493	J231935.43-022903.3	18.980 ± 0.024	17.582 ± 0.005	16.922 ± 0.005	16.653 ± 0.006	16.580 ± 0.009
56805	J232519.88+140339.7	18.051 ± 0.014	16.461 ± 0.004	15.867 ± 0.005	15.570 ± 0.005	15.405 ± 0.006

Table B1. Individual radial velocity measurements ($H\alpha$).

NLTT	BJD (2450000+)	v_r (km s^{-1})	NLTT	BJD (2450000+)	v_r (km s^{-1})	NLTT	BJD (2450000+)	v_r (km s^{-1})
00082	5129.54679	38.9 ± 2.0	12758	5127.81251	83.5 ± 2.5	17662A	5173.80780	43.2 ± 1.0
00082	5129.56148	38.5 ± 4.9	12758	5127.82371	86.6 ± 2.5	17662A	5173.82249	41.2 ± 1.2
00082	5129.58041	40.9 ± 2.9	12758	5127.83957	80.8 ± 1.7	17662B	5173.80780	43.2 ± 3.5
00082	5129.59510	44.8 ± 2.2	12758	5127.85088	81.3 ± 3.1	17662B	5173.82249	53.1 ± 3.3
00347	5129.61463	4.4 ± 1.5	12758	5159.62116	110.2 ± 2.7	17874	5177.75553	36.6 ± 3.6
00347	5129.62932	5.5 ± 1.8	12758	5159.63236	122.9 ± 10.1	17874	5177.77055	35.4 ± 2.0
00347	5129.64781	12.2 ± 1.1	12758	5159.65188	118.7 ± 5.0	17874	5177.79091	37.2 ± 1.3
00347	5129.66248	11.8 ± 1.3	12758	5159.66308	122.5 ± 4.7	17874	5177.80594	37.2 ± 2.8
02886	5119.58441	77.4 ± 10.9	12796	5168.62568	62.9 ± 2.9	21913A	5174.82596	98.1 ± 10.8
02886	5119.59978	78.4 ± 10.0	12796	5168.64034	65.6 ± 2.6	21913A	5174.84064	94.9 ± 7.2
02886	5119.61616	82.0 ± 10.5	12796	5211.66185	47.4 ± 2.0	23966	5219.70931	66.7 ± 1.5
02886	5119.63153	89.0 ± 11.5	12796	5211.67653	49.2 ± 2.7	23966	5219.72400	64.3 ± 2.8
03080	5160.56711	22.3 ± 1.3	13015	5126.84079	-91.9 ± 6.0	23966	5219.74182	51.6 ± 2.0
03080	5160.57254	21.8 ± 1.3	13015	5126.85721	-92.9 ± 4.9	23966	5219.75649	51.1 ± 2.0
03080	5167.54764	29.0 ± 1.2	13015	5145.76540	-119.5 ± 9.3	24406	5230.72715	119.0 ± 1.4
03080	5167.55306	29.2 ± 0.9	13015	5145.78181	-131.9 ± 3.5	24406	5230.74356	119.9 ± 2.3
03080	5186.58826	35.0 ± 1.5	13015	5159.68154	-119.3 ± 10.6	24406	5236.62599	131.0 ± 3.0
03080	5186.59368	34.2 ± 0.9	13015	5159.69795	-134.7 ± 4.7	24406	5236.64241	120.3 ± 1.5
03471	5129.68300	30.0 ± 1.4	13471	5205.72033	46.6 ± 1.7	24406	5241.64830	123.4 ± 2.0
03471	5129.69768	30.3 ± 1.4	13471	5205.73617	41.5 ± 2.1	24406	5241.66470	118.4 ± 2.8
03471	5130.56893	27.8 ± 1.3	13471	5221.66551	34.6 ± 2.3	31473	5227.72301	133.6 ± 2.2
03471	5130.58360	27.0 ± 1.9	13471	5221.68134	30.4 ± 2.6	31473	5227.73769	130.2 ± 4.3
04615	5130.60388	50.2 ± 3.5	13471	5227.68215	53.7 ± 3.5	31473	5228.74950	90.1 ± 2.5
04615	5130.62030	48.6 ± 2.4	13471	5227.69800	52.2 ± 2.2	31473	5236.65995	118.5 ± 2.1
04615	5130.64061	57.4 ± 2.3	13532	5120.67703	112.2 ± 8.0	31473	5236.67463	106.0 ± 1.1
04615	5130.65704	50.2 ± 2.0	13532	5120.69175	138.8 ± 19.2	31473	5260.60814	91.9 ± 2.1
05503	5167.57190	25.5 ± 2.2	13532	5221.62982	126.3 ± 7.9	31473	5260.62282	92.1 ± 19.2
05503	5167.58659	26.9 ± 0.9	13532	5221.64451	106.4 ± 17.2	31473	5261.60819	129.7 ± 4.6
05503	5168.55934	24.3 ± 2.4	13532	5228.59386	107.3 ± 6.2	31473	5261.62287	122.2 ± 1.8
05503	5168.57403	31.6 ± 2.8	13532	5228.60854	115.7 ± 11.2	32785	5227.83769	36.6 ± 4.4
05814	5119.65517	62.2 ± 2.1	13755	5174.69455	71.8 ± 2.5	32785	5227.84659	34.0 ± 5.6
05814	5119.67558	68.9 ± 2.3	13755	5174.70924	73.3 ± 2.3	32785	5260.64423	44.9 ± 6.8
06559	5202.54687	69.0 ± 3.1	13755	5174.72599	82.5 ± 2.3	32785	5260.66007	25.9 ± 6.3
06559	5202.56328	66.0 ± 1.3	13755	5174.74067	80.0 ± 2.2	32785	5262.65007	39.9 ± 5.6
06559	5221.54948	91.5 ± 0.5	14491	5220.64861	46.5 ± 1.2	32785	5262.66590	32.5 ± 7.8
06559	5221.56590	88.9 ± 1.9	14491	5220.66502	45.4 ± 2.7	33503	5260.68062	111.8 ± 1.2
06794	5120.63607	86.6 ± 1.4	14491	5220.68455	53.2 ± 3.0	33503	5260.69530	111.3 ± 1.4
06794	5120.65248	87.4 ± 1.8	14491	5220.70096	45.0 ± 2.2	35570	5260.71462	-0.6 ± 0.9
06794	5221.58891	74.3 ± 2.2	15882	5226.70469	34.8 ± 1.5	35570	5260.72930	-5.9 ± 2.3
06794	5221.60533	73.0 ± 1.2	15882	5226.72052	31.7 ± 17.2	50161	5164.55701	2.4 ± 17.2
07051	5119.69701	90.5 ± 7.8	15882	5226.74176	40.9 ± 1.5	50161	5164.57343	6.9 ± 16.9
07051	5119.71169	81.1 ± 4.3	15882	5226.75758	31.0 ± 5.3	51252	5163.55031	18.3 ± 1.7
08432	5165.57389	66.1 ± 2.8	15882	5228.63304	37.2 ± 3.1	51252	5163.56673	19.2 ± 1.6
08432	5165.59036	63.9 ± 3.2	15882	5228.64888	37.3 ± 1.8	56045	5186.55285	19.7 ± 2.1
08432	5228.55214	64.8 ± 2.3	15882	5228.71117	39.2 ± 2.1	56045	5186.56926	19.0 ± 1.8
08432	5228.56855	67.8 ± 2.3	15882	5228.72700	33.9 ± 3.6	56257	5165.53139	40.6 ± 1.9
09940	5159.72102	79.2 ± 4.4	15957	5174.76253	108.0 ± 3.0	56257	5165.54607	40.7 ± 2.4
09940	5159.73744	72.4 ± 5.7	15957	5174.77720	106.9 ± 5.9	56257	5181.55685	55.9 ± 1.4
09940	5159.75445	76.7 ± 4.6	15957	5174.79403	113.7 ± 2.4	56257	5181.57154	54.7 ± 2.4
09940	5159.77088	92.8 ± 4.9	15957	5174.80871	100.3 ± 2.3	56493	5181.59296	88.6 ± 5.4
12758	5127.78391	92.3 ± 2.0	17486	5119.76508	122.5 ± 2.3	56493	5181.60880	69.6 ± 11.8
12758	5127.79512	91.1 ± 1.8	17486	5119.77977	127.4 ± 2.5			